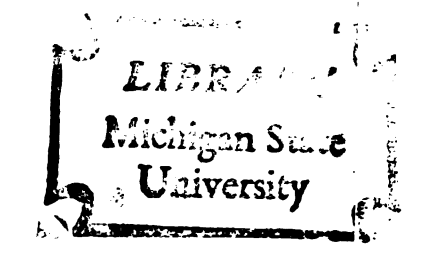
A STRENGTH CRITERION FOR GRANULAR MATERIALS WITH SPECIAL REFERENCE TO ARCH FORMATIONS IN SEEDS

Thesis for the Degree of Ph. D.
MICHIGAN STATE UNIVERSITY
Robert Dean Fox
1968



This is to certify that the

thesis entitled

A STRENGTH CRITERION FOR GRANULAR MATERIALS WITH SPECIAL REFERENCE TO ARCH FORMATIONS IN SEEDS

presented by

Robert Dean Fox

has been accepted towards fulfillment of the requirements for

Ph.D. degree in Agricultural Engineering

Major professor

Date January 10, 1968

ABSTRACT

A STRENGTH CRITERION FOR GRANULAR MATERIALS WITH SPECIAL REFERENCE TO ARCH FORMATIONS IN SEEDS

By Robert Dean Fox

The gravity flow of granular material is limited by the formation of bridges or arches in the material as it flows through chutes or bin outlets. These arches may stop the flow and disrupt the process using the granular material. As an introduction to the study of arch formations in agricultural materials, observations were made of the arch systems formed in pea beans, oats and raw sugar beet seeds. These observations were made to determine the properties of the granular materials which affected the strength of the material for forming arches. The materials were selected for their differences in kernel size, shape and expected potential for forming arches.

All arches were formed over a long narrow slit in the bottom of a flat-bottomed, model bin. Tests were made of the effect of the following factors on the arching characteristics of the materials:

- 1. compacting the seeds by vibrating the bin
- 2. applying a vertical load to the upper surface of the material in the bin
- 3. changing the moisture content of the material
- 4. changing the orientation of the particles.

After these studies, it was determined that several properties not included in commonly used yield criteria do indeed affect the arching

strength of a material. Thus a yield criterion was developed which was dependent not only on the internal friction and cohesive strength of the material, but also on the angle of the shearing plane, the particle shape and the particle orientation in the mass of material.

This criterion was developed for a specific stacking arrangement of ellipsoidal particles. The stacking arrangement was made as general as possible, while still maintaining mathematical workability. The yield criterion was based on the assumption that the forces acting along the failure surface in the material are transmitted across this surface only at the contact points between the individual particles on each side of the failure plane. The particulate nature of the material was expressed in a yield criterion which could be used in the mathematical formulations commonly used for continuous materials.

The yield criterion developed in this study has the following properties:

- 1. The material has a minimum strength at a shearing angle which is determined from the particle shape and stacking arrangement.
- 2. The maximum strength occurs for shearing in a plane parallel to the shortest axis of the particles.
- 3. If the friction or cohesion between particles in the material increases, or if the void ratio of the material decreases, the effect of the angle of shearing decreases.

ROBERT DEAN FOX

Although no data was collected to test the yield criterion directly, the expected failure derived from the yield criterion agrees well with the failures observed in the arch tests.

Approved Major Professor

Approved Department Chairman

A STRENGTH CRITERION FOR GRANULAR MATERIALS WITH SPECIAL REFERENCE TO ARCH FORMATIONS IN SEEDS

 $\mathbf{B}\mathbf{y}$

Robert Dean Fox

A THESIS

Submitted to
Michigan State University
in partial fulfillment of the requirements
for the degree of

DOCTOR OF PHILOSOPHY

Department of Agricultural Engineering

ACKNOWLEDGEMENTS

Throughout this study Dr. S. Persson has been a constant source of advice, suggestions and inspiration; I was fortunate to have Dr. Persson for my Major Professor.

I am also grateful to the other members of the graduate committee for their advice and guidance during the program; these members were:

- Dr. L. Malvern, Professor of Metallurgy, Mechanics and
 Materials Science
- Dr. J. Boyd, Professor of Agricultural Engineering, and
- Dr. R. Hamelink, Assistant Professor of Mathematics.

During the early stages of this study Dr. F. Buelow served as advisor; his counsel during this period was very helpful.

TABLE OF CONTENTS

				Page
AC	KNOW	LEDGE	MENTS	ii
LIS	T OF	FIGURE	s	vi
LIS	T OF	TABLES	5	ix
C ha	pter			
I.	INTR	ODUCT	ON	1
	1.1.	Definiti	ion of the Problem	1
		1.1.1.	The objectives of the study	2
	1.2.	Prelim	inary Considerations	3
		1.2.1.	Selection of materials	3
		1.2.2.	Definition of terms	3
		1.2.3.	Observations of stable arch systems	5
	1.3.	Selection	on of an Approach	8
II.	THE	месна	NICS OF THE PROBLEM	10
	2.1.	The Ma	terial as a Mass of Discrete Particles	10
		2.1.1.	Review of literature	10
		2.1.2.	Outline of approach	17
		2.1.3.	The arrangement of the particles in a stack	18
		2.1.4.	The normal and tangential forces acting on a failure surface	26
		2.1.5.	A discussion of the yield criterion	39
	2.2.	The Co	ntinuous Mass Approach	43
		2.2.1.	Review of literature	43
		2.2.2.	Application of the continuous mass approach	50

Cha	pter			Page
	2.3.	The Fo	rces Acting in Particle Arches	53
		2.3.1.	Review of literature	53
		2.3.2.	The two-dimensional parabolic arch	54
		2.3.3.	Computation of the parabola shape factor "m"	57
		2.3.4.	Forces acting in an arch	59
III.	THE	FACTO	RIAL STUDY	65
	3.1.	The Te	sting System	65
		3.1.1.	Apparatus	65
		3.1.2.	Test procedures	65
		3.1.3.	Materials used in the tests	66
	3.2.	Observ	ations of Arch Systems	68
		3.2.1.	Orientation of particles	68
		3.2.2.	Primary-secondary arch systems	69
		3.2.3.	Other observations	72
	3.3.	Factors	Influencing Arching	73
	3.4.	Gap Wie	dth-Particle Size Relationship	74
		3.4.1.	Review of literature	74
		3.4.2.	Results of tests	77
		3.4.3.	Comparison with the results of Section 2.3.4	78
	3.5. Effect of Applying a Vertical Load to the Grain Mass			80
		3.5.1.	Review of literature	80
		3.5.2.	Effect of applying a vertical load to pea beans	83
		3.5.3.	Effect of applying a vertical load to oat kernels	88

Cha	Page		
		3.5.4. Effect of applying a vertical load to sugar beet seed	90
	3.6.	Effect of Relative Humidity of the Ambient Air on Arch Formation	92
IV.	CLOS	SURE	93
	4.1.	Conclusions	93
	4.2.	Suggestions for Future Study	93
REFERENCES			

LIST OF FIGURES

Figure		Page
1.1.	The materials used in this study	4
1.2.	A typical stable arch system in pea beans	6
1.3.	A typical stable arch system in oat kernels	6
1.4.	A stable arch system in compacted sugar beet seed	9
2.1.	Deflection of the supporting base under a wedge of granular material (Trollope)	10
2.2.	Force system acting in a mass of rhombohedrally packed disks (Trollope)	12
2.3.	Forces acting on slipping cylinders on a granular slope (Laszlo)	12
2.4.	Section view of a model particle stack (Ross-Isaacs)	14
2.5.	Forces acting on a particle in the particle stack (Ross-Isaacs)	14
2.6.	The element of volume in a granular mass (Mogami)	16
2.7.	Arrangement of particles in the first two tiers of the particle stack $(m = n = 1) \dots \dots$	20
2.8.	The possible values for δ and η include the shaded area and the line segments AB and BC .	24
2.9.	Arrangement of particles in a unit volume	25
2.10.	Porosity of the particle stack for various values of the stacking constants	27
2.11.	The particle mass showing the a -plane and the failure surface	28
2.12.	Type I contacts along the a -plane with n = 1, m = 0 stacking	30
2.13.	Type II contacts (with one type I) along the a -plane with n = 1, m = 0 stacking	30

Figure		Page
2.14.	Type I and type II contacts along the a-plane with n = 1, m = 1 stacking	31
2.15.	Definition of the "plus" and "minus" directions of movement along the a -plane	29
2.16.	The forces acting on a particle in the left body during incipient minus motion, showing the positive directions for \overline{F}_N and \overline{F}_μ	36
2.17.	The components of the angle β	36
2.18.	The x- and z-components of the unit vectors normal and tangential to the a-plane, for this case	36
2.19.	The forces acting on a particle in the left body during incipient plus motion, showing the positive directions for \overline{F}_N and \overline{F}_μ	36
2.20.	A particle stack showing the α -plane for particles with all type I contacts except the particle in the N^{th} tier	37
2.21.	The effect of the shearing angle on μ_a and the frequency of type II contacts	41
2.22.	The force element used by Janssen	44
2.23.	The force element used by Terzaghi	44
2.24.	A finite square plate with a hole in the center showing the boundary conditions used by Schlack and Little	46
2.25.	The force system in an arched material under an applied vertical load	52
2.26.	An arched material considered as an elastic body	52
2.27.	An arch under a uniform load per unit span	55
2.28.	An arch under a load with a horizontal top	55
2.29.	A parabolic arch formed with an odd number of particles	58
2.30.	The geometry of calculating "m"	58

Figure		Page
2.31.	The force system acting on particles in an arch	61
2.32.	The external forces acting on a three particle arch in equilibrium	63
2.33.	The external forces acting on a five particle arch in equilibrium	64
3.1.	The model bin used in the tests	66
3.2.	Types of primary arches	70
3.3.	Arch shape factors measured by Aytaman	81
3.4.	The load necessary to produce initial arches in 50% of tests with beans, for various depths of material	85
3.5.	Vertical pressure on the bottom of the bin for various depths of beans, computed by three methods	87
3.6.	Effect of the applied load on the formation of stable arch systems in sugar beet seeds	91
3.7.	Effect of relative humidity on the formation of	01

LIST OF TABLES

Table		Page
2.1.	The distribution of volume elements (Mogami) .	16
3.1.	Particle information	67
3.2.	Percent of trials in which stable arch systems formed in beans for various slit widths and strip spacings	71
3.3.	Flow properties of several materials (Brown and Richards)	76
3.4.	Orifice reduction constant for several small seeds (Beverloo, et al.)	77
3.5.	Maximum arch widths for test materials	78
3.6.	Relation between applied load and the formation of initial arches for various depths of oats over a slit width of 0.55 in	89
3.7.	Relation between applied load and the formation of flow arches for various depths of oats over a slit width of 0.55 in	89

I. INTRODUCTION

1.1. Definition of the Problem

A bridge or a stable arch system will be used interchangeably in this study to describe a condition where particles of grain become arranged in a dome-like formation with sufficient strength to support the material above the dome or bridge. A bridge will obviously impede the smooth flow of grain or even stop flow entirely. A stable arch system is most likely to occur at a bin outlet or in a grain chute.

With the increase in the use of automatic materials handling and feeding systems on farmsteads, the problems of arching in grain have increased greatly. Not only has the possibility for arching increased, through the use of more bins, chutes and pipes, but with time clock controlled, automatic feeding systems, the amount of feed delivered to a group of animals could unknowingly be reduced or stopped. This problem is often encountered in milking parlors where a ground ration is stored in a bin above the milking stations and is gravity fed into the individual feeding boxes. Stable arch systems which form over the chutes leading to the feeding boxes require that the operator leave his milking station to break the arches before the milking operation can continue.

Menear and Holdren (1965) found that hay wafers, a relatively new agricultural product, formed a very strong bridge over the outlet in the bottom of a storage bin. These bridges were very difficult to destroy; this important property may limit the acceptance of this material by farmers.

An agricultural material gaining widespread use at the present time is high moisture grain. The British agency NAAS (1967) reported bridging problems in removing high moisture grain from bottomunloading airtight silos, especially if the moisture content of the grain was above 24% or if the grain contained trash.

In situations where the flow rate of granular materials is being controlled by using a narrow opening, bridging can again cause problems. An example of this is the feeding of corn kernels into the slots of the plate of a corn planter. Khan (1966) found that the shape of the floor of the grain box around the plate had an influence on the percentage of plate slots which would fill with seeds.

Other industries have also been plagued for many years with flow stoppages due to bridging materials and are still fighting the problem with many means, such as changing the physical properties of the flow materials (solids conditioning), redesigning the hopper shape, or using air pressure, vibrators, and the old standby, the rubber mallet, to stimulate flow.

1.1.1. The objectives of this study

The objectives of this study were:

- 1. to observe arch formations in granular materials to identify the mechanics of arch building,
- 2. to identify factors which influence the size, structure, and strength of the arch systems,
- 3. to find a relationship between these factors which will explain the formation of arches, with the hope that this information about arches might lead to an insight into a system of preventing or destroying them.

1.2. Preliminary Considerations

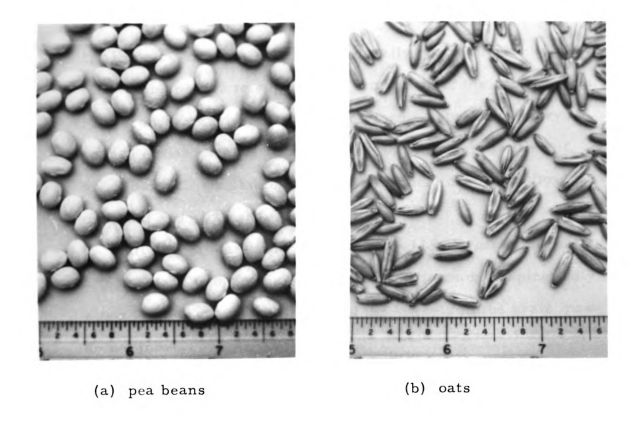
1.2.1. Selection of materials

Before deciding on a theoretical approach, preliminary observations were made of arch systems in different materials. For this preliminary study several decisions about the selection of methods and materials had to be made.

- 1. In order to limit the study to the two dimensional case, the grain bridge was formed over a long narrow slit in the bottom of a flat bottomed bin.
- 2. Pea beans were selected as one of the arching materials because they were approximately spherical in shape and were large enough to make the individual particles in the arch observable (see Figure 1.1 for a picture of the test materials).
- 3. To test the effect of a differently shaped material on arch formation, oats were also selected. The oat kernel is approximately a long, thin cylinder in shape.
- 4. Raw sugar beet seeds were selected as a third test material. They have a somewhat irregular shape with points and corners, but they could be best described as spherical in outline. Sugar beet seeds tend to lock together when compacted; thus they were expected to have a high potential for arching.

1.2.2. Definition of terms

1. Stable arch system - any arrangement of particles over the slit that prevents the flow of material; usually composed of several primary and secondary arches. Figure 1.2 shows a stable arch system in pea beans; note the primary-secondary arch structure.





(c) raw sugar beet seed

Figure 1.1. The materials used in this study.

- 2. Primary arch a short arch, usually perpendicular to the slit which appears to support the remainder of the arch system.
- 3. Secondary arch an arch which forms between primary archs, either parallel to the slit or obliquely across the slit.
- 4. Flow arch a stable arch system which forms in a flowing material and stops the flow.
- 5. Initial arch a stable arch system which forms immediately after the slit is opened and prevents flow from developing; only a few kernels of grain fall out and the kernels in the grain mass do not move.
- 6. Compacted material material compacted by shaking the model bin for 10 seconds; the shaking was done manually, in a direction parallel to the slit length.
- 7. Preloaded material material compacted by applying a load (preload) to the top of the grain column for a short time and removing the load before the slit was opened.
- 8. Constant load the load applied to the grain column and remaining in place until after the slit was opened and the trial run completed.

1.2.3. Observations of stable arch systems

The following observations were made in the apparatus described in Section 3.1, but were discussed here because they directly affected the selection of the theoretical methods used in this study.

The arch systems which formed in pea beans were usually flow arches. The orientation of the particles during flow and their random positioning seemed to bring about the necessary conditions for arch



Figure 1.2. A typical stable arch system in pea beans.

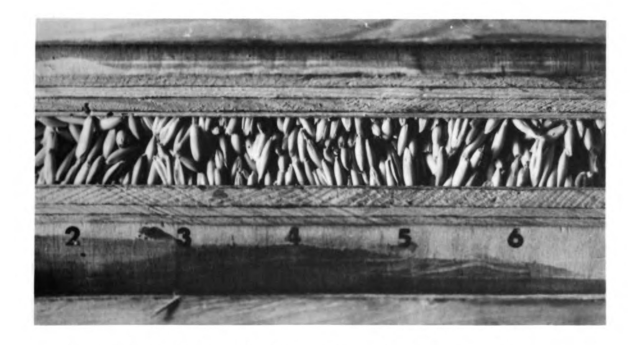


Figure 1.3. A typical stable arch system in oat kernels.

formation. The dimension of a bean which affected arch formation appeared to be its smallest diameter (considering the bean as an ellipsoid). A bean in an arch rarely was positioned with its longest dimension parallel to the arch direction. The primary-secondary arch structure was more pronounced in beans than in the other materials tested (see Figure 1.2). This structure made it apparent that the arch system in beans could not be considered a purely two dimensional problem. Furthermore the stable arch system would form only over slit widths of two particle diameters or less, which meant that only two or three particles made up most primary arches.

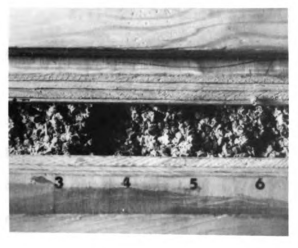
Oat kernels formed mainly initial arch systems; they would form flow arches occasionally but not often. Stable arch systems in oats tended to be very flat and quite uniform along the length of the slit, that is, with very little secondary arch structure (see Figure 1.3). The critical dimension of the oat kernel in the formation of arches seemed to be the length of the kernel. When forming an arch the kernels tended to lie flat (with the long axis parallel to the bottom of the bin) and extended across the slit, being held in place by and at the same time supporting the kernels in higher tiers.

When sugar beet seed was poured loosely into the bin, its arching properties were similar to those of beans. However when the beet seeds were compacted by shaking the bin before opening the slit, their behavior changed considerably. Compacted seeds formed very stable initial arch systems over wide slit widths. These arch systems were so stable that the lower portion of the material, defined as the primary arches in beans, could be removed until the arch had a nearly

smooth cylindrical shape over the entire length of the slit (see Figure 1.4). This arch system appeared to be a series of parallel primary arches placed side by side. In this condition, there seemed to be a thin layer of particles, located within two or three particle diameters of the arch bottom, which were the key to the support of the arch. If a hole was made in this layer, the seeds flowed out rapidly.

1.3. Selection of an Approach

After making these preliminary observations of the materials selected for this study, a model based on the force system between individual particles seemed to provide a more accurate description of the mechanics than one based on the assumption of a continuous material. Thus this study concentrated on trying to find a particle-mass model which would describe the formation of arches in a granular material. However, continuous models have been developed to explain the behavior of granular materials under many different conditions and some of these models were used for comparison with the test results of this study.





(a) as formed

(b) after the lower particles were removed



(c) an arch 2-1/2 in. wide, formed under a surface load of 1 psi.



(d) an end view of (c)

Figure 1.4. A stable arch system in compacted sugar beet seed.

II. THE MECHANICS OF THE PROBLEM

2.1. The Material as a Mass of Discrete Particles

2.1.1. Review of literature

Trollope (1957) studied the stability of a granular wedge under conditions of a single (horizontal) surface constraint (see Figure 2.1). He evaluated the stress distribution within a granular mass under the influence of gravity from an analysis of the static equilibrium of a systematically packed system of mono-sized, smooth, non-frictional, rigid spheres. The necessary stability in such a wedge was satisfied with a unique packing arrangement, the hexagonal rhombohedral. A two-dimensional view of this type of packing is

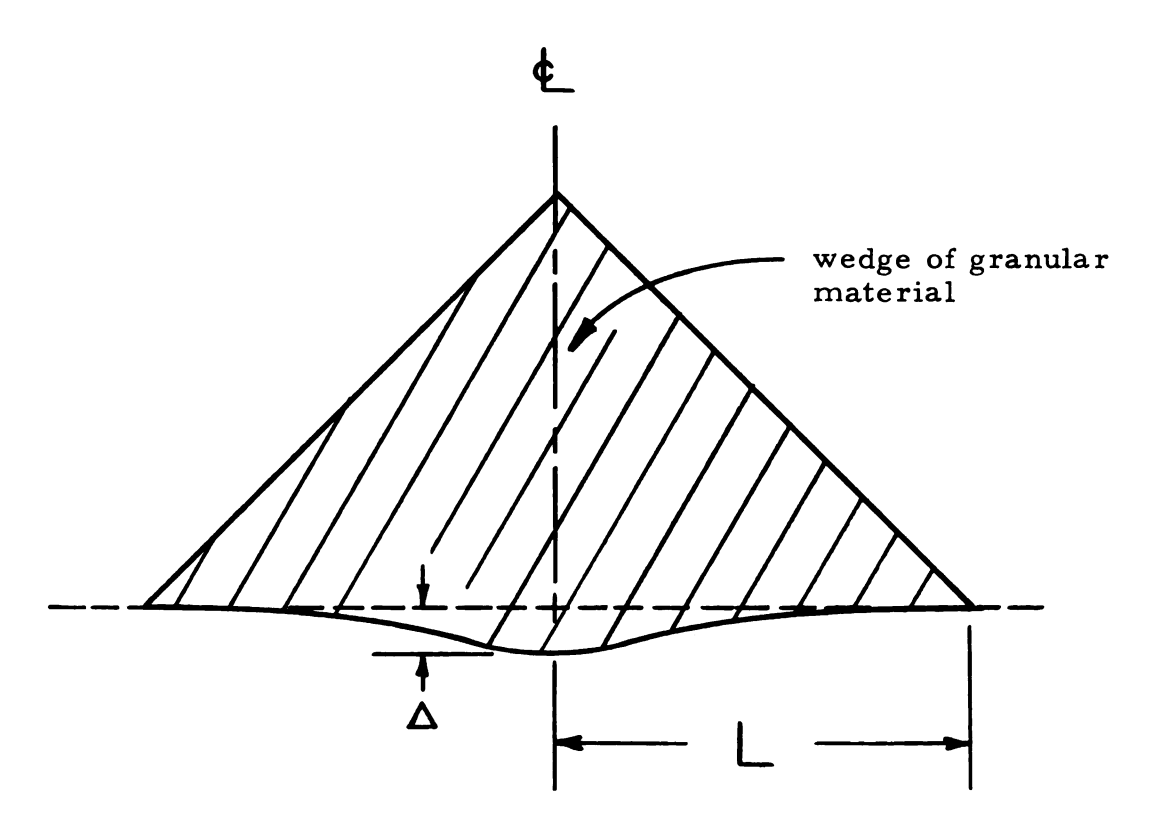


Figure 2.1. Deflection of the supporting base under a wedge of granular material (Trollope).

shown in Figure 2.2. The loading forces, ℓq , mq and nq, acting on the particle considered in this figure were known from the boundary conditions; ℓ , m and n represented integers. The support forces acting on this particle were Z_1 , Z_2 , and X. The two limiting conditions for static equilibrium are also shown in this figure. Trollope defined

$$Z_2 = a' \left[\frac{m+1}{\ell+1} \right] Z_1$$
,

where a' was an "arching factor" which was related to the deflection of the supporting base. No arching occurred over a rigid base but arching occurred if the base was allowed to deflect. The arching factor a' was dependent upon the deflection coefficient of the base (Δ/L) , which is shown in Figure 2.1. Trollope found good agreement between the predicted and measured pressure distribution across the base of laboratory models of sand wedges.

Laszlo (1962) discussed the factors affecting the stability of the particles in the surface layer of a granular slope. Using cylinders and spheres as models, he derived expressions for the forces acting on the surface particles under the action of friction. The force system considered by Laszlo is shown in Figure 2.3. In this figure Q_i was the force acting on the surface particle by the particles in the interior of the mass; all Q-forces acted at an angle θ . P_i was the force acting on a surface particle by the next lower surface particle; all P-forces acted at α , the slope angle of the stack.

μ was the coefficient of friction between the particles.

In this force system, P_i must be greater than Q_i to maintain the equilibrium of moments acting on the particles. The force on any

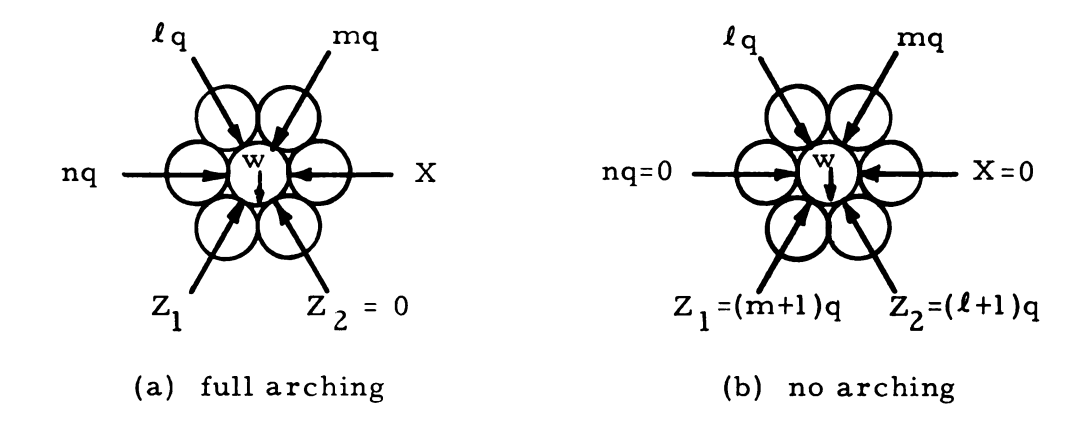


Figure 2.2. Force systems acting in a mass of rhombohedrally packed disks (Trollope).

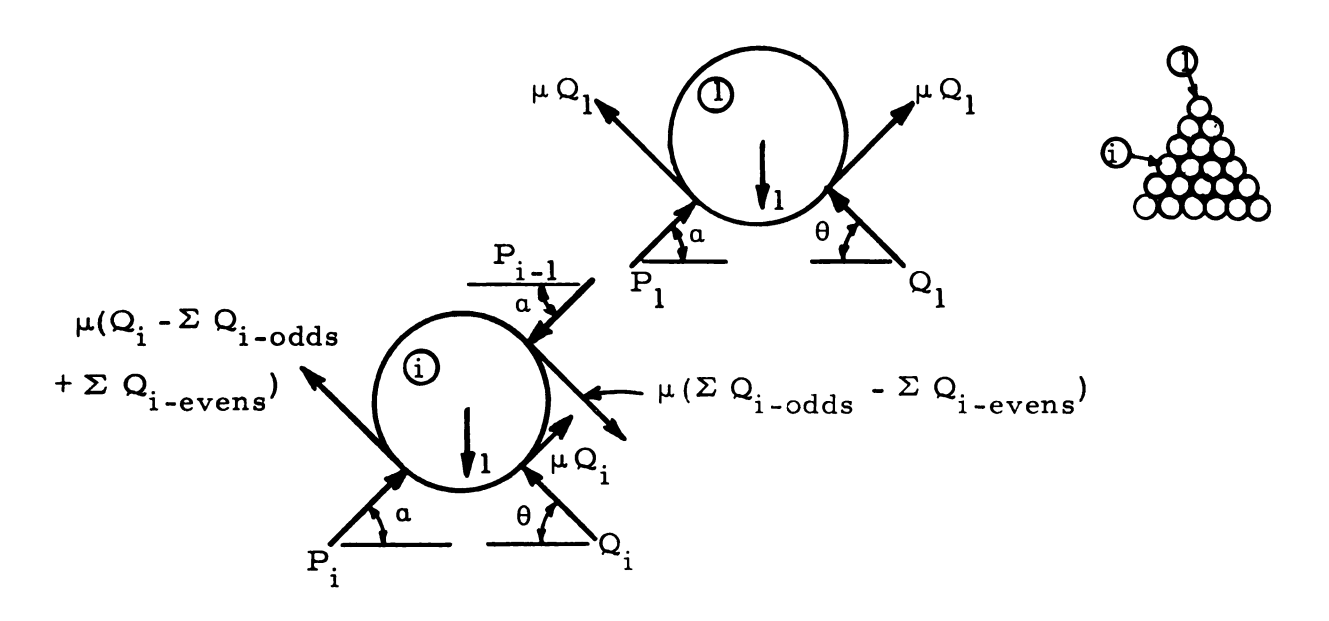


Figure 2.3. Forces acting on slipping cylinders on a granular slope (Laszlo).

particle was found in terms of the force balance of the uppermost particle and the number of particles in the surface layer. Laszlo seems to have made an error in deriving the final expressions for Q_i and P_i .

Ross and Isaacs (1961) used the force system between particles to derive expressions for the total vertical force on the bottom of a bin and for the vertical and lateral pressures acting in a bin. They assumed the particles were inelastic spheres, then defined a characteristic particle size, \overline{d} , and stacking angle θ for each material These characteristic values were determined from the porosity and specific density of the materials. They considered only the static case where friction could be neglected. The stacking system used for their calculations is shown in Figure 2.4. The stacking arrangement in the yz-plane was exactly like the arrangement in the xz-plane shown in Figure 2.4. Thus four θ -axes pass through each particle. The length of a θ -axis is upward from the particle to the boundary of the particle mass. Figure 2.5 shows the forces acting on an individual particle in the center of the stack. Each of four particles above act with a force m on this particle and each of four particles below support this particle with a force F. By summing the forces acting on the particles in successive tiers, Ross and Isaacs found the total vertical force exerted by a particle on its support to be

$$F_{TV-n} = \overline{L}_{\theta} w/\overline{d}$$
 ,

where \overline{L}_{θ} is the average length of the four θ -axes and w is the

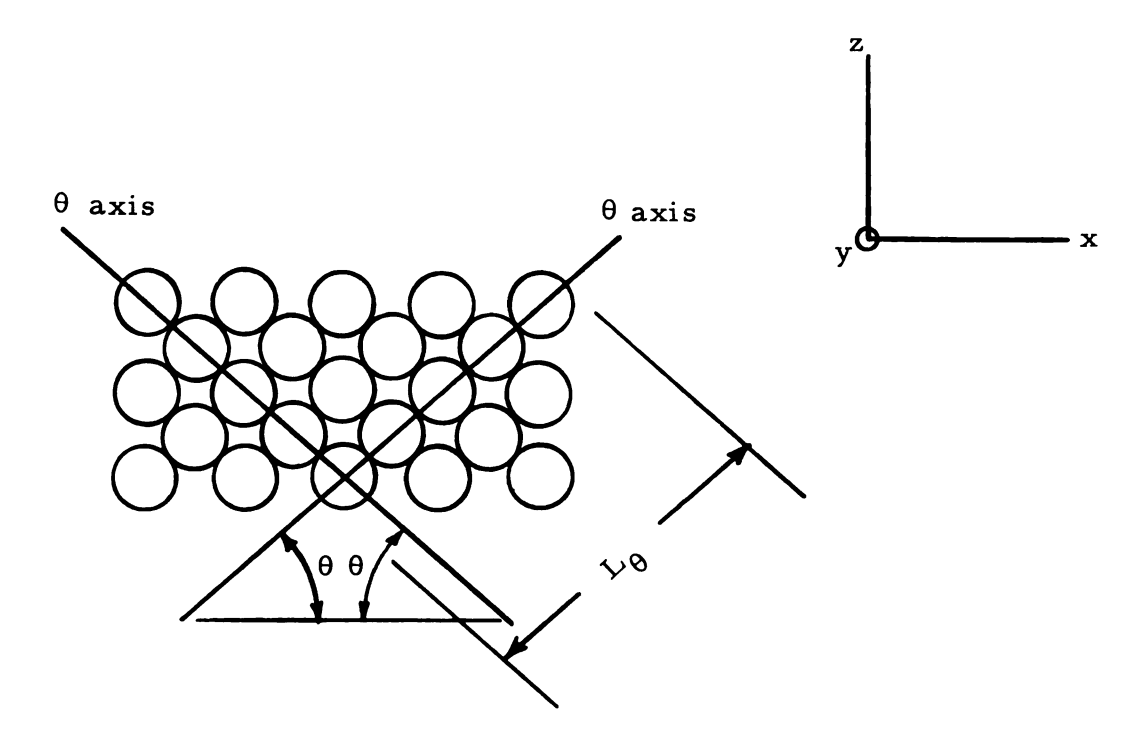


Figure 2.4. Section view of a model particle stack (Ross-Isaacs).

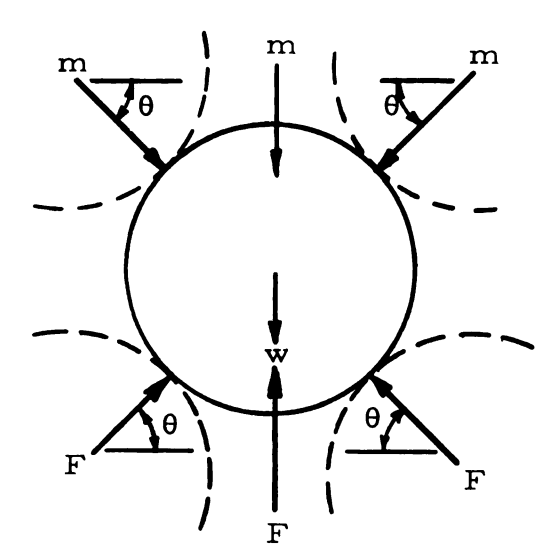


Figure 2.5. Forces acting on a particle in the particle stack (Ross-Isaacs).

weight of each particle. To find the forces acting in a particle stack enclosed by a retaining wall, Ross and Isaacs assumed that the retaining walls acted as a weightless particle column, that is, the wall supported the particles as if the particle stack continued beyond the wall, but did not apply any additional force to the lower particles. The total force acting on the bin floor was found to be

$$F_{\text{floor}} = \frac{J^2 \text{ wh}}{4 \overline{d}^3 \cos^2 \theta \sin \theta} - \frac{J \text{ wh}^2}{8 \overline{d}^3 \cos \theta \sin^2 \theta}$$
 (2.1)

where J is the width of the square bin and h is the height of the grain in the bin. This equation is valid for grain heights up to J tan θ . They found good agreement between the values calculated from Equation (2.1) and experimental measurements. The equations for the vertical and lateral pressures acting in a bin were:

$$P_{floor} = \frac{\overline{L}_{\theta} w}{4 \overline{d}^3 \cos^2 \theta}$$
 (2.2)

and

$$P_{\text{wall}} = L_{\theta}^{\dagger} \cdot \frac{w(1 + \cos \theta)}{8 d^{3} \sin^{2} \theta \cos \theta}$$
 (2.3)

where L_{θ}^{\dagger} is the length of the θ -axis in the xz-plane. Ross and Isaacs showed that the lateral pressure measured by Saul (1953) agreed closely with Equation (2.3), but the vertical pressure on the bin floor measured by Saul was 10% to 15% higher than calculated from Equation (2.2).

Mogami (1965) derived a relationship between the statistical distribution of the void ratios and the principal stresses in a granular mass. He considered the granular mass as a series of elements such as is shown in Figure 2.6. He classified these elements according to

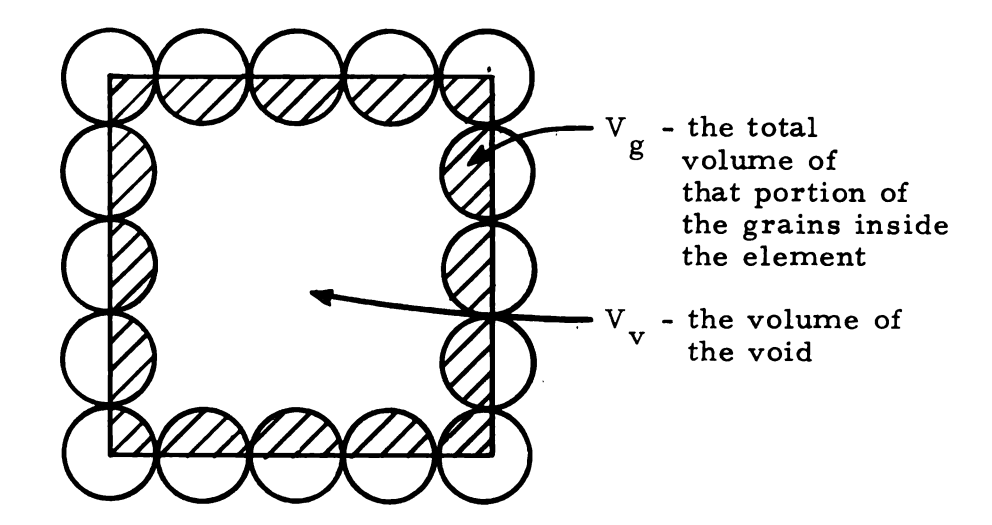


Figure 2.6. The element of volume in a granular mass (Mogami).

their void ratios and volumes as is shown in Table 2.1, where e_1, e_2, \ldots, e_n were the void ratios in ascending order, v_i (i=1,2,...,n) were the total volume of the elements having the void ratio e_i and N_i (i=1,2,...,n) were the total volume of the grains contained in the elements which had the void ratio e_i , in terms of the number of grains. Mogami then applied the methods of statistical mechanics to this system and found an expression for the probability of the state in terms of the

Table 2.1. The distribution of volume elements (Mogami)

$${\bf e}_1 \ {\bf e}_2 \ {\bf e}_3 \ \cdots \ {\bf e}_n$$
 ${\bf v}_1 \ {\bf v}_2 \ {\bf v}_3 \ \cdots \ {\bf v}_n$
 ${\bf N}_1 \ {\bf N}_2 \ {\bf N}_3 \ \cdots \ {\bf N}_n$

void ratios and their standard deviation. Then by relating the volumetric strain in plane stress to the change in void ratio, he derived expressions for the principal stresses in terms of the void ratio, the maximum shearing strain and a suitable constant. In a later paper Mogami (1966) compared the constant, k', which he calculated from published data of triaxial and plane shear tests in sand and found k' to be consistent within each set of tests.

2.1.2. Outline of approach

During the initial part of this study, several attempts were made to describe the forces acting between individual particles in a mass of material; particularly particles in grain arches. These methods were not successful because the force system acting between the particles in the mass involved many possible combinations of forces and force directions. Thus, before the system could be solved, such assumptions had to be made that the validity of the solution was highly questionable. Many of these problems would be overcome if the influence of the mass surrounding the critical area could be included while still recognizing the particle nature of the failure area. This could be achieved if the particle nature of the system could be incorporated into a continuous mass type of description.

The following development was made to find a yield criterion of this kind. From continuum mechanics was utilized the concept of an imaginary plane through the particle mass, separating the mass into two bodies. Taken over a sufficiently large area of this plane, the resultants of the forces are assumed to be proportional to the area. The internal force state in the original mass can be represented by forces

perpendicular and tangential to the imaginary plane.

From particle mechanics were taken the concepts that forces are transmitted between bodies at the contact points, that the directions of the forces should be related to the common normal to the bodies at the points of contact and that there exists a relationship between the normal and tangential contact forces.

The two approaches are combined by the assumption that appropriate components of the resultant of the contact forces in the particle picture are the same as the unit area forces in the continuum representation.

The yield criterion was designed to consider both pure friction and cohesion between the particles, and also the orientation of the particles. The following sections discuss the assumed particle stacking arrangement and the force system between the particles necessary to arrive at the yield condition.

2.1.3. The arrangement of the particles in a stack

The stacking arrangement of the particles in a mass of material determines the points of contact between the particles and the direction of the normal at the contact points; this essentially establishes the force system which acts between the particles. The assumptions made in selecting the packing system for this study and the properties resulting from this arrangement of particles are given below.

Assumptions:

- 1. The particles had an ellipsoidal shape with the two minor axes equal (the length of the minor axes = 2b).
- 2. All particles were oriented with their longest axis parallel to the x-axis (the length of the major axis = 2a).

- 3. The particles were arranged in a systematic manner with equidistant spacing; the spacing was independent of position in the mass.
- 4. Each particle was in contact with all adjacent particles.

Figure 2.7 shows the arrangement of particles used in the following discussion. Four stacking arrangements which satisfy the above conditions are possible. They are:

- a simple rectangular arrangement with a center spacing of
 a in the x-direction and 2b in the y- and z-directions.
- 2. a body centered rectangular arrangement with a center spacing of $2\delta a$ in the x-direction, $2\eta b$ in the y-direction and a z-distance dependent on δ and η (this is the arrangement shown in Figure 2.7, the z-distance is shown in this figure but the derivation of this distance will be given later).
- 3. an arrangement which has face centered particles in the xz-plane and is rectangular in the yz-plane. The center spacings in this arrangement are $2\delta a$ in the x-direction, 2b in the y-direction and a z-distance determined by δ .
- 4. an arrangement which has face centered particles in the yz-plane and is rectangular in the xz-plane. The center spacings in this arrangement are 2a in the x-direction, $2\eta b$ in the y-direction and a z-distance determined by η .

To include these four arrangements in one mathematical formulation, the stacking constants m and n were used. The only possible values for m and n are 0 and 1. These constants are used in the description of the distance between the centers of particles in

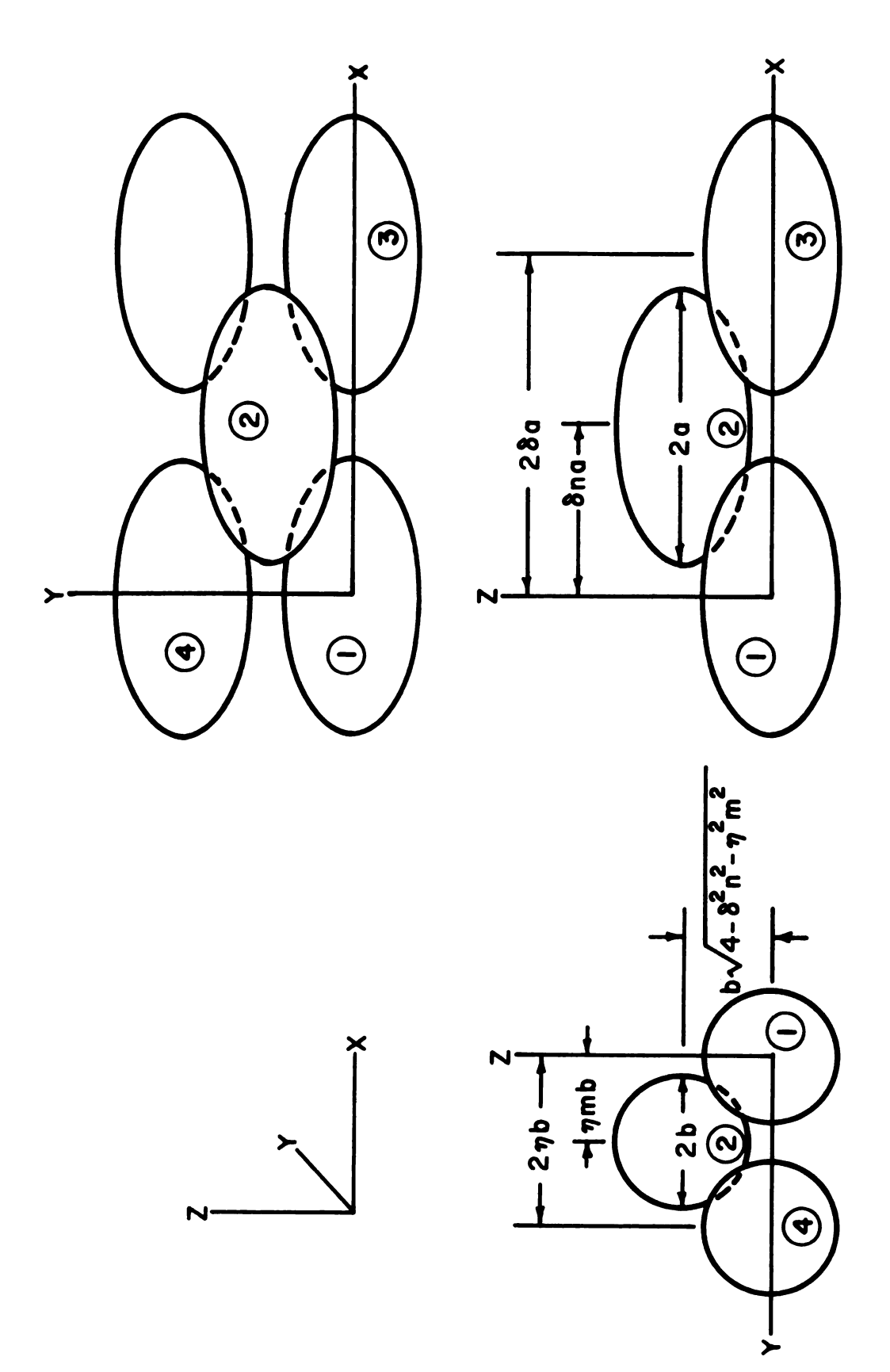


Figure 2.7. Arrangement of particles in the first two tiers of the particle stack (m = n = 1).

adjacent tiers. In Figure 2.7, the center spacing between particles 1 and 2 in the x-direction is $n\delta a$ and the center spacing between these particles in the y-direction is $m\eta b$. Thus the four arrangements mentioned above are given by the following values of m and n:

Arrangement	m-value	n-value
1	0	0
2	1	1
3	0	1
4	1	0

These four arrangements were made more general by including the stacking variables δ and η . These variables allow the distance between the center of particles in the same tier to be varied. The distance in the x-direction between the centers of particles 1 and 3 in Figure 2.7 is $2\delta a$. The y-distance between the centers of particles 1 and 4 is $2\eta b$. The minimum value for these variables is $\delta = \eta = 1$.

The stacking constants and variables are used only in the xand y-directions. The particles in higher tiers are assumed to be
supported by the lower particles, so that the z-distance between
centers can be calculated if the x- and y-distances are known.

Using this method, the distance between the centers of any particle can be calculated from the position of the adjacent particle. Thus for particles in the same tier

$$h_3 = h_1 + 2\delta a$$
 and $k_4 = k_1 + 2\eta b$

where (h, k) is the center of each particle shown in Figure 2.7, and for particles in adjacent tiers

$$h_2 = h_1 + n\delta a$$
 and $k_2 = k_1 + m\eta b$.

The particles in tier three were placed directly above those in tier one; tier four was exactly like tier two, etc.

The following method was used to calculate the z-coordinate of the center of particle 2 (see Figure 2.7). The x- and y-coordinates of the center of this particle were fixed at (a δ n, b η m). Let the desired z-coordinate be c, then the equations of particles 1 and 2 are

$$\frac{x^2}{a^2} + \frac{y^2}{b^2} + \frac{z^2}{b^2} = 1 ,$$

and (2.4)

$$\frac{(x - a \delta n)^2}{a^2} + \frac{(y - b \eta m)^2}{b^2} + \frac{(z - c)^2}{b^2} = 1.$$

These two particles touch only at the point (x₁, y₁, z₁), where they have a common tangent plane. The direction numbers of the normals at this contact point were found by taking the gradient of Equations 2.4. These direction numbers were:

$$\frac{\mathbf{x}_1}{a}$$
; $\frac{\mathbf{y}_1}{b^2}$; $\frac{\mathbf{z}_1}{b}$, and

$$\frac{x_1 - a \delta n}{a^2}$$
; $\frac{y_1 - b \eta m}{b^2}$; $\frac{z_1 - c}{b^2}$,

respectively.

The normals are parallel, but have opposite directions.

Therefore

$$-\frac{x_1}{a^2} = K \frac{(x_1 - a\delta n)}{a^2} ,$$

$$-\frac{y_1}{b^2} = K \frac{(y_1 - b\eta m)}{b^2} , \text{ and}$$
$$-\frac{z_1}{b^2} = K \frac{(z_1 - c)}{b^2} .$$

In order to satisfy Equations 2.4, K = 1, and the point of contact becomes:

$$(x_1, y_1, z_1) = (\frac{a\delta n}{2}, \frac{b\eta m}{2}, \frac{c}{2}).$$
 (2.5)

(These results could also be found from symmetry arguments.)
From Equations 2.4,

$$c = b\sqrt{4 - \delta^2 n^2 - \eta^2 m^2} . (2.6)$$

Thus the center of particle 2 becomes:

$$(a\delta n, b\eta m, b\sqrt{4 - \delta^2 n^2 - \eta^2 m^2})$$
.

The values of δ and η must be restricted in size, for if they become too large, the particles in tier three will touch the particles in tier one without touching the particles in tier two. Thus the z-coordinate of the center particle 5 (see Figure 2.9) must be greater than 2b, giving,

$$2b\sqrt{4-\delta^2n^2-\eta^2m^2} > 2b$$

or

$$\delta^2 n^2 + \eta^2 m^2 < 3$$
.

This, in combination with the conditions that $\delta \ge 1$, $\eta \ge 1$, m = 1 or 0, n = 1 or 0, gives the possible values of δ and η shown in Figure 2.8.

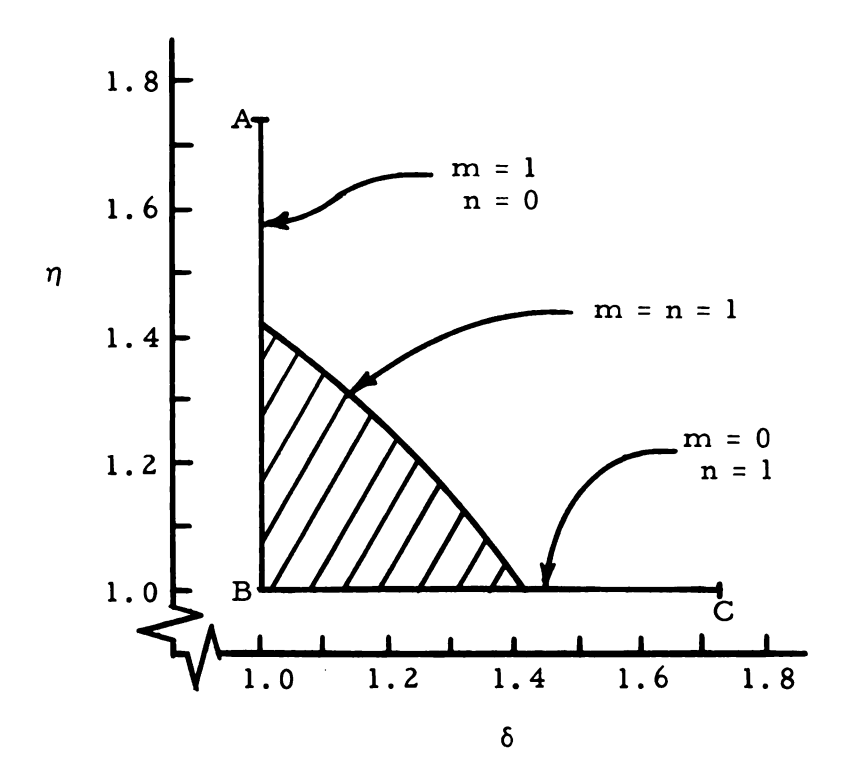


Figure 2.8. The possible values for δ and η include the shaded area and the line segments AB and BC.

To find the porosity of this packing system, consider the parallelepiped outlined by the heavy lines in Figure 2.9. This parallelepiped contains the volume of two particles. Thus the volume of the material is $8\pi ab^2/3$, and the porosity of this system is;

porosity =
$$1 - \frac{\text{volume of material}}{\text{total volume}}$$
, or

porosity = $1 - \frac{\pi}{3 \delta \eta \sqrt{4 - \delta^2 n^2 - \eta^2 m^2}}$. (2.7)

The porosity of this stacking system for various values of the stacking numbers are shown in Figure 2.10. The system is symmetric with respect to δ and η . Although Figure 2.10 is drawn for δ with curves for various values of η , the same relationships would hold if

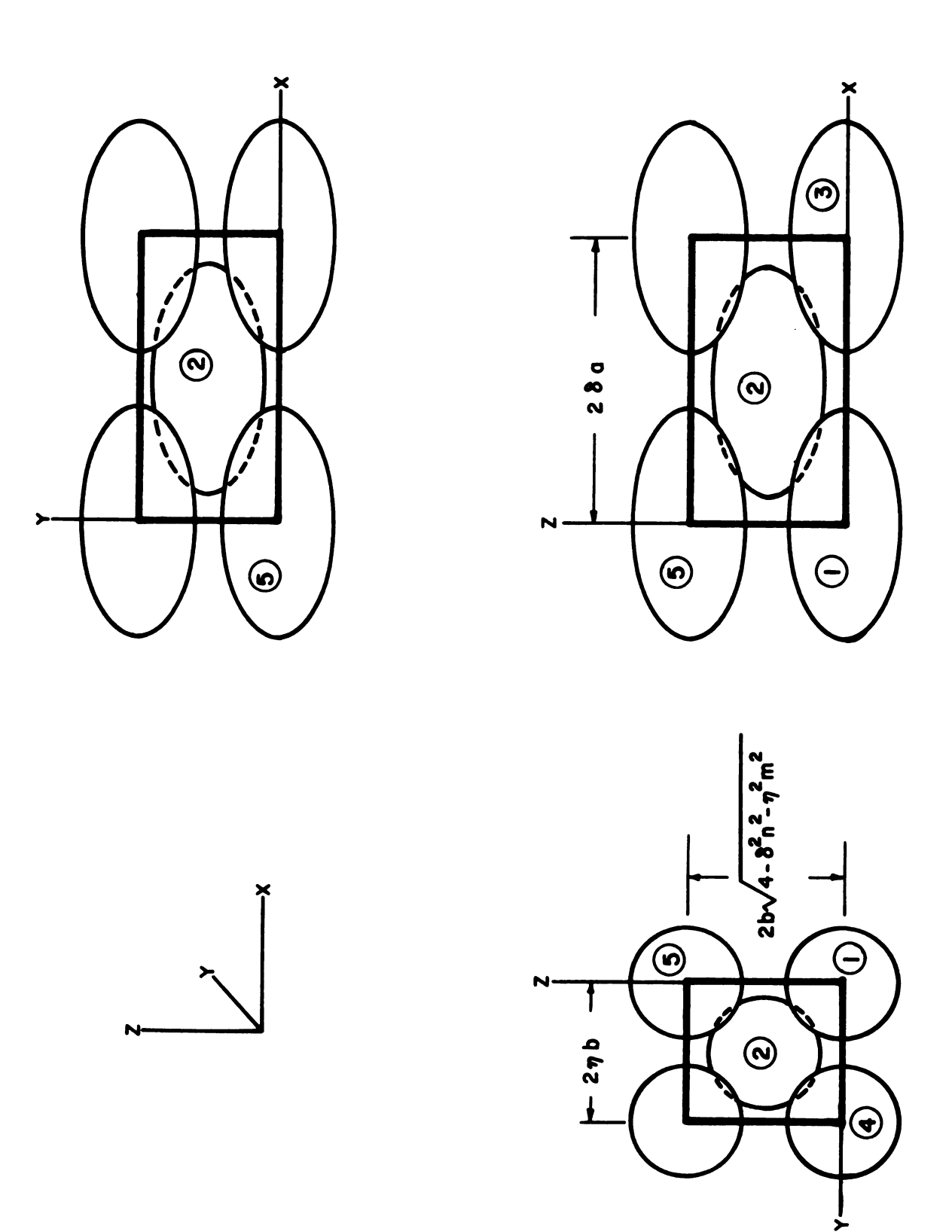


Figure 2.9. Arrangement of particles in a unit volume.

the δ and η symbols were exchanged.

As can be seen from the diagram, the minimum porosity of 0.26 is achieved for $\delta = \eta = 1$, n = m = 1. The maximum porosity of 0.47 occurs for n = m = 0, which fixes $\delta = \eta = 1$.

As a comparison, Ross and Isaacs (1961) measured the porosity of several materials: their results were:

material	porosity
shelled corn	0.39
oats	0.50
soybeans	0.39
wheat	0.39

All of these porosity values, except oats, fall within the range given in Figure 2.10. From measurements of the bulk density of loose and compacted oats, it appears that the porosity of compacted oats would be approximately 0.46. Thus the stacking model developed here may be used to describe the porosity of the materials quite accurately.

2.1.4. The normal and tangential forces acting on a failure surface

The failure was assumed to occur along a plane containing the y-axis and passing through the particle mass at an angle a to the z-axis (see Figure 2.11). Any movement in the mass involved the body on the left side of the a-plane sliding over the body on the right side. This implied that motion in the y-direction was zero. This a-plane divided the mass of particles into two bodies; this discussion considers the forces which act between these two bodies.

Because the mass was made up of particles which were assumed to remain intact, the boundary between the two bodies was not exactly

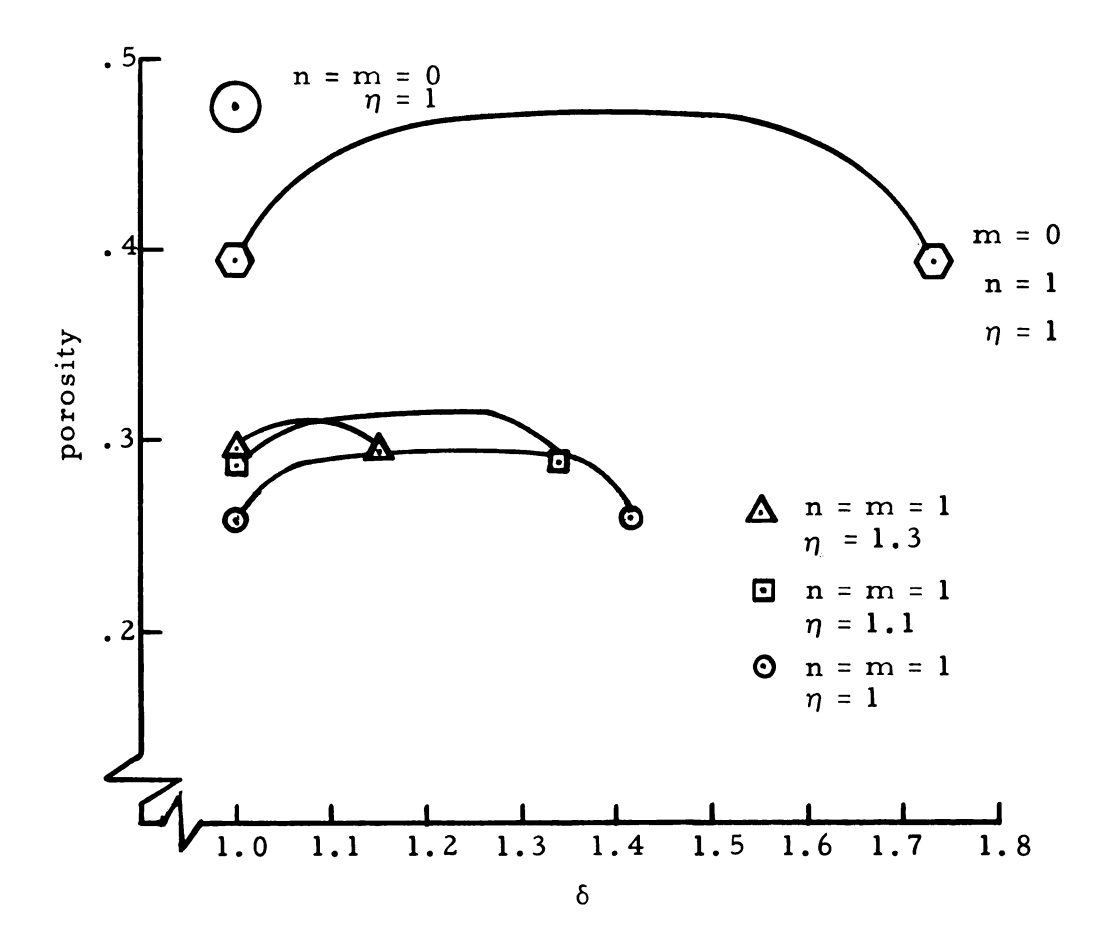


Figure 2.10. Porosity of the particle stack for various values of the stacking constants.

a plane, but appeared to zigzag across the a-plane following the particle boundaries. The position of the center of the particle determined the dividing line between the two bodies; any particle whose center was on or to the left of the a-plane was considered to be in the left body and any particle whose center was to the right of the a-plane was in the right body (see Figure 2.11).

The only contact points between the particles which affected the forces between the two bodies were those along the zigzag boundary.

All other forces occurred within the bodies and were not considered.

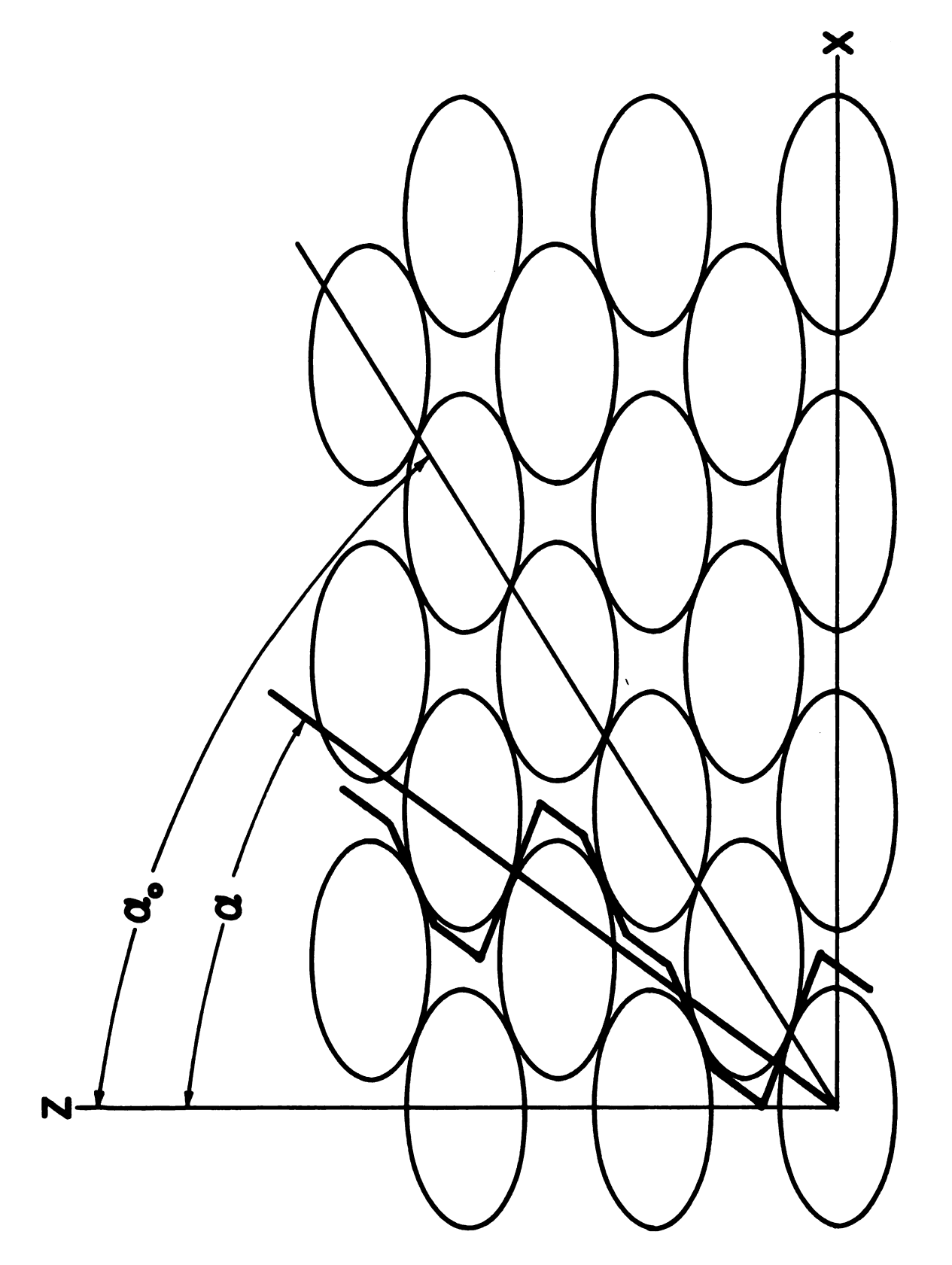


Figure 2.11. The particle mass showing the α -plane and the failure surface.

Figures 2.12, 2.13 and 2.14 show close-ups of the contact points between several particles.

All forces between the two bodies act in one of two planes; these two kinds of contact planes were defined as type I and type II. Figures 2.12 and 2.13 show type I and type II contacts for the case m = 0, n = 1; however as is shown in Figure 2.14, the case m = n = 1 can be treated with the same type of contact forces by using the position equations developed in Section 2.1.3. For ease of visualization, all future figures will show the case n = 1, m = 0, but the equations will be derived for the general case of all combinations of n and m equal 0 or 1.

The direction of movement of the body to the left of the a -plane over the body to the right affects the force system between the bodies. Figure 2.15 defines "plus" and "minus" directions of motion.

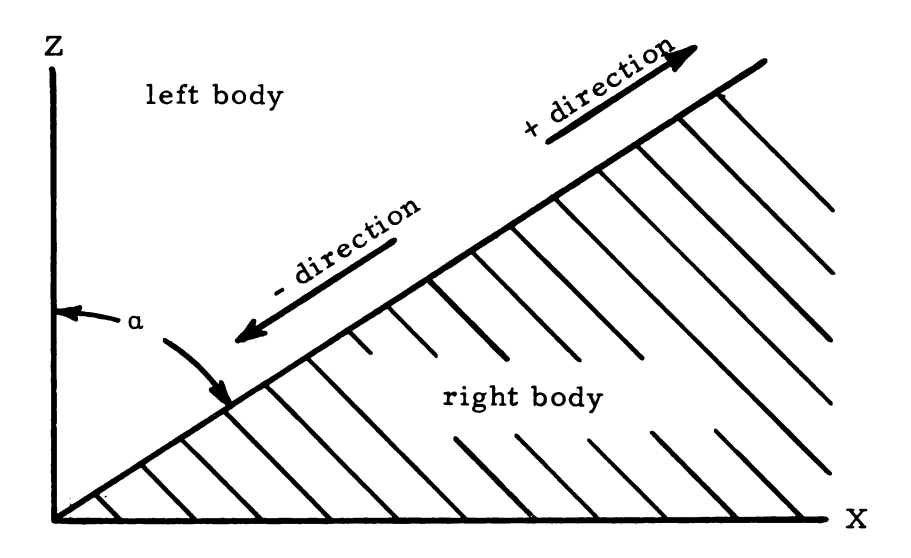


Figure 2.15. Definition of the "plus" and "minus" directions of movement along the a -plane.

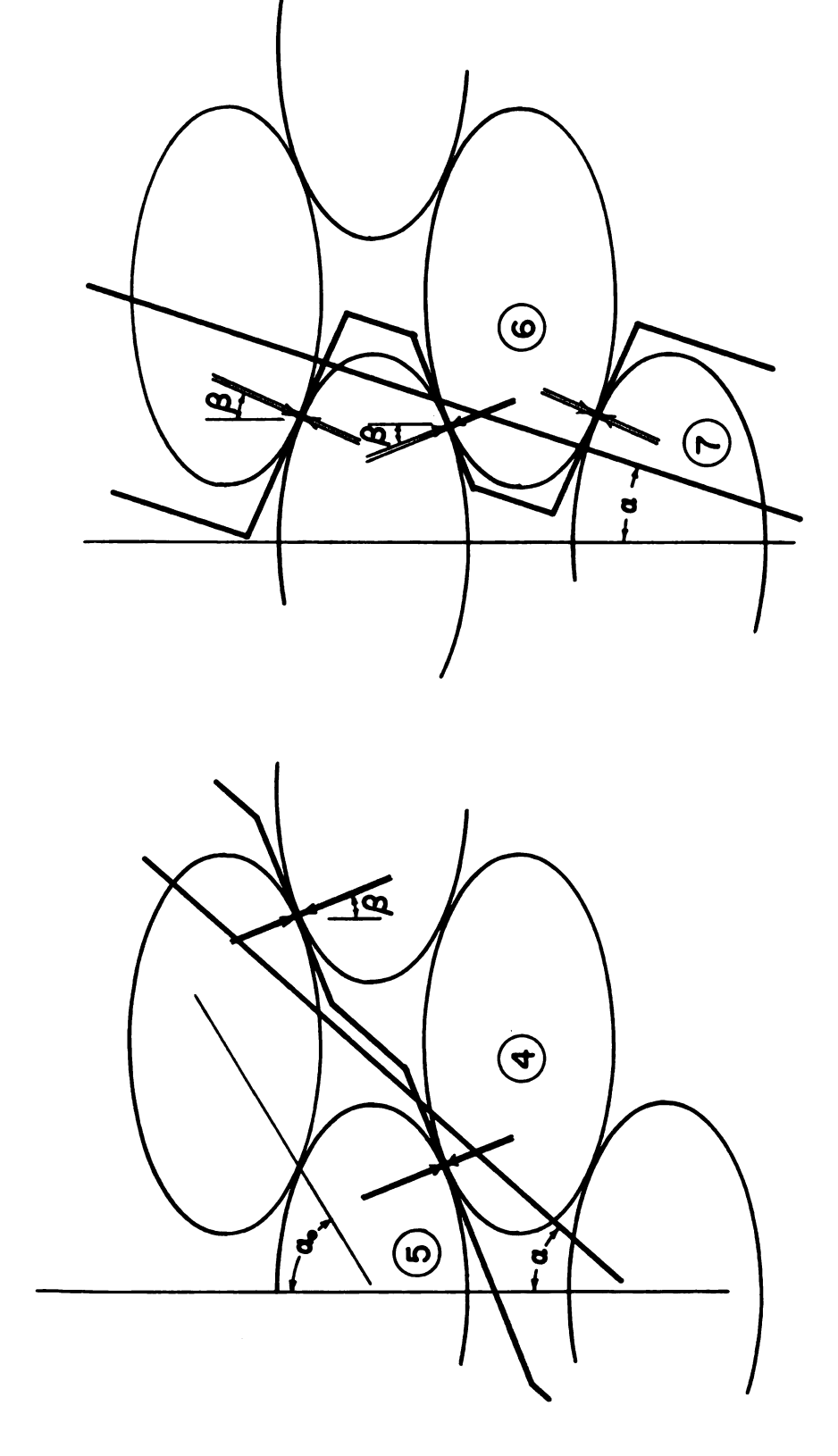


Figure 2.12. Type I contacts along the α-plane with n = 1, m = 0 stacking.

Figure 2.13. Type II contacts (with one type I) along the α -plane with n=1, m=0 stacking.

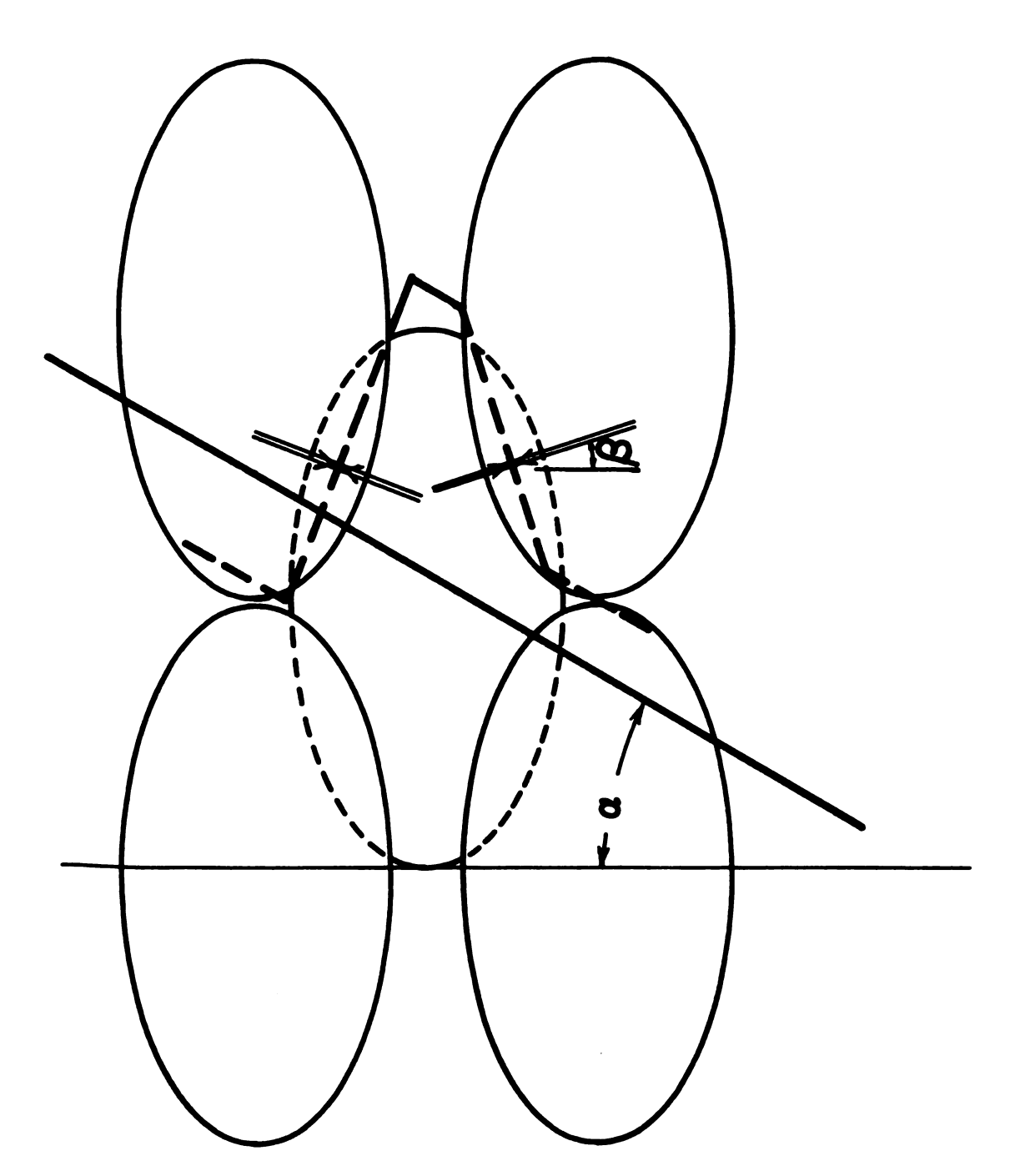


Figure 2.14. Type I and type II contacts along the α -plane with n=1, m=1 stacking.

Looking at Figure 2.13 again, it can be seen that after a very small "plus" movement, the type I contact forces no longer act, so that all of the resisting force takes place at type II contacts. On the other hand, for "minus" movement, only the type I contact forces are active. Therefore, the force system acting for each type of motion can be treated separately. If the movement between bodies is large, it is obvious that displacement of particles would have to occur, however this study will limit its discussion to incipient movement so that the particles can be assumed to retain their position in the particle stack.

In the previous discussion, it was shown that minus motion of the left body was associated with the forces acting between particles at type I contacts and that plus motion of the left body was associated with the forces acting between particles at type II contacts. These two types of movement will be considered separately.

The case of minus movement - type I contacts will be discussed first. The total force acting at a type I contact will be determined and then the components of this force in the directions normal (n) and tangential (t) to the a-plane will be calculated. The force acting at the type I contact was taken to be the force that a particle in the right body exerted on a particle in the left body.

Consider the type I contact between particles 4 and 5 in Figure 2.12. The unit vector in the direction normal to particle 5 at this point is

$$\vec{N} = \left(-\frac{\lambda \delta n}{C_5}, \frac{\eta m}{C_5}, \frac{C_3}{C_5}\right)$$

where

$$\lambda = \frac{b}{a}, C_3 = \sqrt{4 - \delta^2 n^2 - \eta^2 m^2},$$

and

$$C_5 = \sqrt{4 + (\lambda^2 - 1) \delta^2 n^2}$$
.

Thus the normal force acting on particle 5 in the left body at one type I contact is:

$$\vec{F}_{N} = F_{N} \left(-\frac{\lambda \delta n}{C_{5}} \vec{i} + \frac{\eta m}{C_{5}} \vec{j} + \frac{C_{3}}{C_{5}} \vec{k} \right) . \qquad (2.8)$$

This force is only one of a pair of forces which act on each particle in each (projected) contact plane. In this case there is a particle directly behind particle 4 which acts on particle 5 from the other side with a normal force,

$$\vec{F}_N = F_N \left(-\frac{\lambda \delta n}{C_5} \vec{i} - \frac{\eta m}{C_5} \vec{j} + \frac{C_3}{C_5} \vec{k} \right)$$

so that the two normal forces acting in each contact plane are balanced in the y-direction. Because only motion in the xz-plane is being considered, only one normal force of each force-pair in a contact plane will be considered in the following discussion.

The friction force, \overrightarrow{F}_{μ} , acts in the same plane as the motion and opposes this motion. In this case, it would act in the xz-plane, i.e., perpendicular to the \overrightarrow{j} direction. The friction force also must act in the plane tangent to the particles at the contact point, i.e., perpendicular to the normal force \overrightarrow{F}_{N} . Thus \overrightarrow{F}_{μ} will act in the direction of $-(\overrightarrow{N}\times\overrightarrow{j})$. Normalizing this resulting vector and taking

the magnitude of the friction force as $\mu\,F_N$, \overline{F}_μ for minus motion becomes:

$$\vec{F}_{\mu} = \mu F_{N} \left(\frac{C_{3}}{C_{4}} \right) + \frac{\lambda \delta n}{C_{4}} (2.9)$$

where,

$$C_4 = \sqrt{C_3^2 + (\lambda \delta n)^2} = \sqrt{C_5^2 - \eta^2 m^2}$$
.

Figure 2.16 shows the forces at a type I contact, acting in the directions which will be considered positive for this case. From the figure, it is apparent that the normal force in Equation 2.8 and the friction force in Equation 2.9 were acting in the positive direction. The total force acting in the xz-plane at a type I contact at incipient minus motion is:

$$(\overrightarrow{F}_T)_{xz} = (\overrightarrow{F}_N + \overrightarrow{F}_{\mu})_{xz}$$
,

which can be written:

$$\vec{F}_{T} = F_{N} \left(-\frac{\lambda \delta n}{C_{5}} + \frac{\mu C_{3}}{C_{4}} \right) \vec{i} + \left(\frac{C_{3}}{C_{5}} + \frac{\mu \lambda \delta n}{C_{4}} \right) \vec{k}$$
 (2.10)

Defining the angle between $(\vec{F}_N)_{xz}$ and the z-axis as β , (see Figure 2.12), i.e., β = arc tan $\frac{\lambda \delta n}{C_3}$, as is shown in Figure 2.17, gives:

$$\overrightarrow{F}_{T} = F_{N} \left[\left(-\frac{C_{4}}{C_{5}} \sin \beta + \mu \cos \beta \right) \overrightarrow{i} + \left(\frac{C_{4}}{C_{5}} \cos \beta + \mu \sin \beta \right) \overrightarrow{k} \right].$$
(2.11)

The unit vectors normal and tangential to the α -plane are \vec{n} = (-cos α , 0, sin α) and \vec{t} = (sin α , 0, cos α), (see Figure 2.18).

The components of \overrightarrow{F}_T in the normal and tangential directions are $\overrightarrow{F}_T \cdot \overrightarrow{n}$ and $\overrightarrow{F}_T \cdot \overrightarrow{t}$. Thus the total force on the α -plane becomes:

$$\vec{F}_{T\alpha} = (\vec{F}_{T} \cdot \vec{n}) \vec{n} + (\vec{F}_{T} \cdot \vec{t}) \vec{t} , \text{ or}$$

$$\vec{F}_{T\alpha} = F_{N} \left[\left\{ \frac{C_{4}}{C_{5}} \sin (\alpha + \beta) - \mu \cos (\alpha + \beta) \right\} \vec{n} + \left\{ \frac{C_{4}}{C_{5}} \cos (\alpha + \beta) + \mu \sin (\alpha + \beta) \right\} \vec{t} \right]. \quad (2.12)$$

Now define an angle γ ; μ = $K\sin\gamma$ and $\frac{C_4}{C_5}$ = $K\cos\gamma$. Introducing these expressions into Equation 2.12 gives:

$$\vec{F}_{T\alpha} = F_N K \left[\sin (\alpha + \beta - \gamma) \vec{n} + \cos (\alpha + \beta - \gamma) \vec{t} \right].$$
 (2.13)

Let μ_{α} be the ratio of the magnitudes of the tangential component to the normal component acting on the α -plane. Then μ_{α} for minus motion becomes:

$$\mu_{\alpha,-I} = \cot (\alpha + \beta - \gamma) . \qquad (2.14)$$

In the same way, μ_{α} can be computed for the plus motion - type II contact case. Figure 2.19 shows the positive directions for the forces acting at a type II contact. In this case, two regions were considered separately, $\alpha < \beta$ and $\alpha > \beta$. This was necessary so that the friction force would always resist the movement of the left body. The positive tangential direction along the α -plane was defined as $\overrightarrow{t} = (-\sin \alpha, 0, -\cos \alpha)$. Then, making the same calculations as for the minus movement case, the ratio μ_{α} for positive motion was found to be:

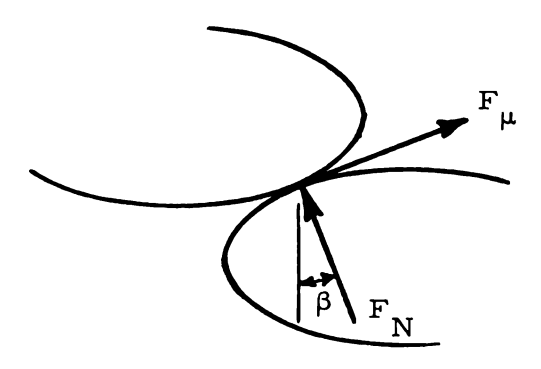


Figure 2.16. The forces acting on a particle in the left body during incipient minus motion, showing the positive directions for \overrightarrow{F}_N and \overrightarrow{F}_μ .

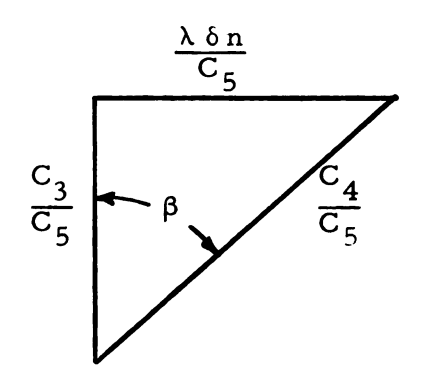


Figure 2.17. The components of the angle β .

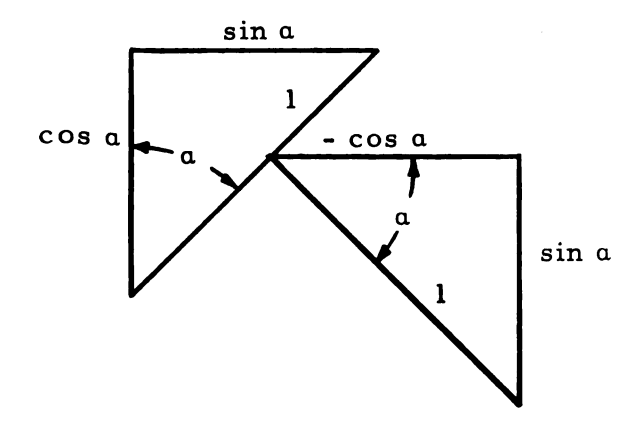


Figure 2.18. The x- and z-components of the unit vectors normal and tangential to the a-plane, for this case.

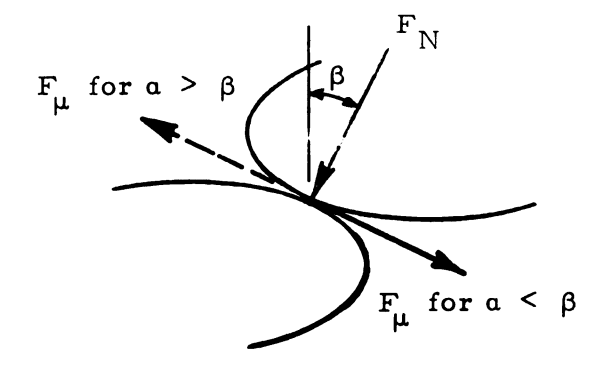


Figure 2.19. The forces acting on a particle in the left body during incipient plus motion, showing the positive directions for \overline{F}_N and \overline{F}_μ .

$$\mu_{\alpha,+II} = \cot (\beta - \alpha - \gamma)$$
 (2.15)

where γ is positive for $\alpha < \beta$ and negative for $\alpha > \beta$.

A discussion of the regions of validity of these equations (2.14 and 2.15) along with numerical values of μ_{Ω} are given in Section 2.1.5.

The relationship between the angle $\,\alpha\,$ and the number of type I and type II contacts was considered next. From Figure 2.11, it is apparent that for $\alpha=0^{\circ}$, 50% of the contacts are of each type, but that for $\alpha=\alpha_{\circ}$, 100% of the contacts are type I. The value of α for the case where all contacts between the particles in the two bodies are type I except for one particle in the top tier is shown in Figure 2.20. There is always one contact for each tier of particles and a type II contact will

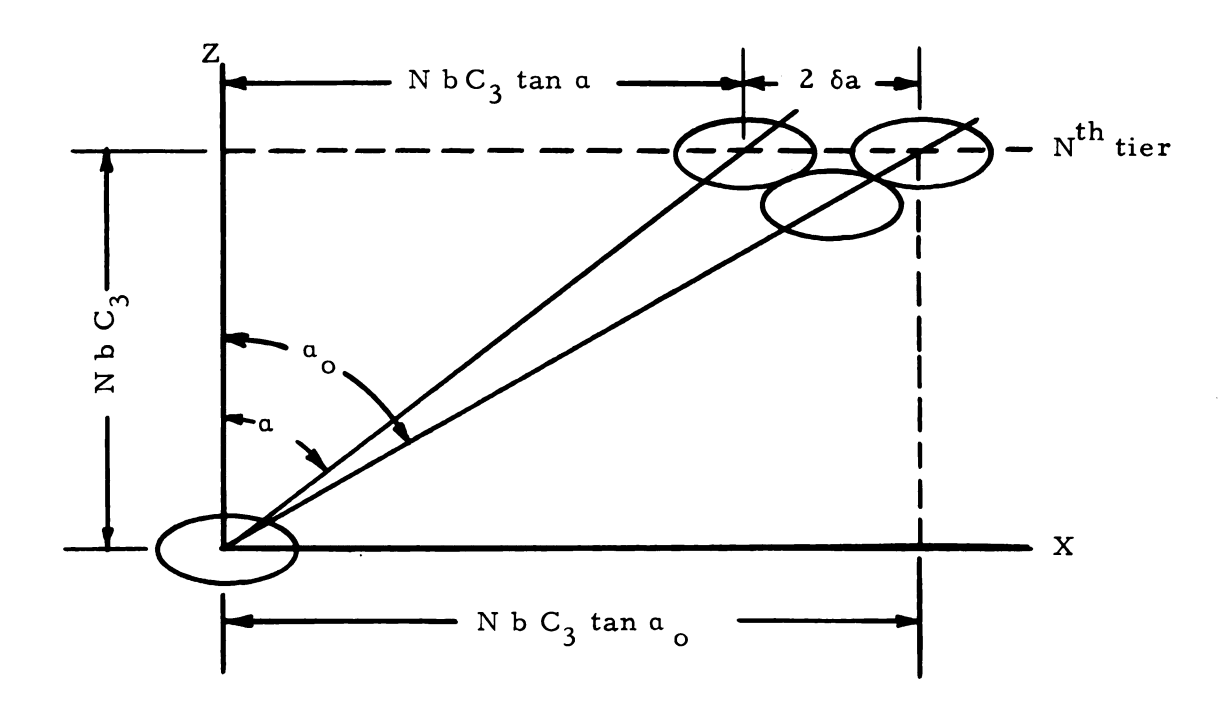


Figure 2.20. A particle stack showing the a-plane for particles with all type I contacts except the particle in the Nth tier.

occur only when the α -plane passes through or to the left of the center of a particle. In Figure 2.20, α was chosen so that the α -plane passed through the center of the first particle to the left of the α -particle in the Nth tier.

From Figure 2.20, $2\delta a = N b C_3 \tan \alpha_0 - N b C_3 \tan \alpha$. Since there is only one type II contact in this case, the fraction of contacts which are type II is 1/N. It follows from the above expression that the frequency of type II contacts is:

$$f_{II} = \frac{1}{N} = \frac{\lambda C_3 (\tan \alpha_0 - \tan \alpha)}{2 \delta}$$
.

Now tan $\alpha_0 = \frac{\delta}{\lambda C_3}$, so $f_{\Pi} = \frac{1}{2} \left(1 - \frac{\tan \alpha}{\tan \alpha}\right)$ for $(0 \le \alpha \le \alpha_0)$.

The remainder of the contacts are type I, so

$$f_{I} = 1 - f_{II} = \frac{1}{2} \left(1 + \frac{\tan \alpha}{\tan \alpha}\right)$$
, for $\left(0 \le \alpha \le \alpha_{0}\right)$,

where f_{I} and f_{II} are the frequency of the type I and II contacts.

Although this solution was developed for the special case of only one type II contact, the same construction can be used for the α -plane passing through the center of any particle in the N^{th} tier.

Because the length of the section along the α -plane is N b $C_3/\cos\alpha$, the number of contacts per unit length becomes:

$$N_{I} = \frac{1}{2 b C_{3}} (\cos \alpha + \frac{\sin \alpha}{\tan \alpha})$$
, $N_{II} = \frac{1}{2 b C_{3}} (\cos \alpha - \frac{\sin \alpha}{\tan \alpha})$, (2.16)

where N_{I} and N_{II} are the number of each type of contact per unit length along the α -plane.

This development would be more general if an interparticle cohesive frictional force was included, because most materials exhibit some cohesive property. This cohesive force can be included in the friction force; thus the magnitude of the friction force becomes, $|\overrightarrow{F}_{\mu}| = \mu \, F_N + F_c \,, \text{ where } F_c \, \text{ is the apparent cohesion. Making this addition to the previous derivations will change the μ-term in the definition of <math display="inline">\gamma$ to $(\mu + \frac{F_c}{F_N})$.

2.1.5. A discussion of the yield criterion

The ratio μ_{α} , of the tangential force acting on the α -plane to the normal force acting on the α -plane, is an expression for the failure strength of a material. When the failure criterion is written as $F_{t\alpha} = \mu_{\alpha} F_{n\alpha} \quad , \quad \text{it is similar in form to the Coulomb yield criterion.}$ Although it may not be obvious from Equations 2.14 and 2.15, μ_{α} is a function of the stacking arrangement, the particle shape, the angle of the failure plane through the mass and the internal friction and cohesion of the material.

The expressions obtained for μ_α in Equations 2.14 and 2.15 are not defined for all combinations of the angles α , β and γ . The following discussion will point out these critical values.

Case 1. Minus motion - type I contacts

This case is valid only for $0 \le \alpha \le 90^\circ - \beta$. For $\alpha < 0$, this case is equal to case 2 for $-\alpha$, due to symmetry. For $\alpha > 90^\circ - \beta$, the contact force will become negative.

$$\mu_{\alpha,-I} = \infty$$
 for $0 \le \alpha \le \gamma - \beta$.

Case 2. Plus motion - type II contacts

This case is valid mainly for $0 \le \alpha \le \beta$. The lower limit applies for the same reason given in case 1. For $\alpha > \beta$ only a very small movement can take place before both type II and type I contacts are established.

$$\mu_{\alpha,+II} = \infty$$
 for $\beta - |\gamma| \le \alpha \le \beta + |\gamma|$,

because at $\alpha=\beta$ the tangential component of \overrightarrow{F}_T is perpendicular to the (projected) contact surface.

This summary, together with the illustration given in Figure 2.21, show that $\mu_{\alpha,+II}$ is not a suitable measure of the yield strength of a material during incipient plus movement. However, it was shown in the previous section that as α increases, the frequency of type II contacts along the α -plane decreases (see Figure 2.21). As α becomes larger, the tangential force acting along the α -plane will be concentrated on a small number of particles and will probably cause the particles to move out of their stacking positions. This violates one of the assumptions made earlier. If small movements in the particles with type II contacts occur, the locus for $\mu_{\alpha,+II}$ would likely be similar to the minus movement case.

On the other hand, for minus movement, $\mu_{\alpha,-I}$ gives reasonable results whenever $\alpha > \gamma - \beta$. Thus this yield criterion can be used only for the case of minus movement and when $\alpha > \gamma - \beta$. To show the relationship between α and μ_{α} , a specific case was considered. A plot of μ_{α} for α -values between 0 and α_{o} is shown in Figure 2.21, for the case when m=0, $\eta=1$, n=1, $\delta=1$, $F_{c}=0$, $\lambda=0.5$, and $\mu=0.1$.

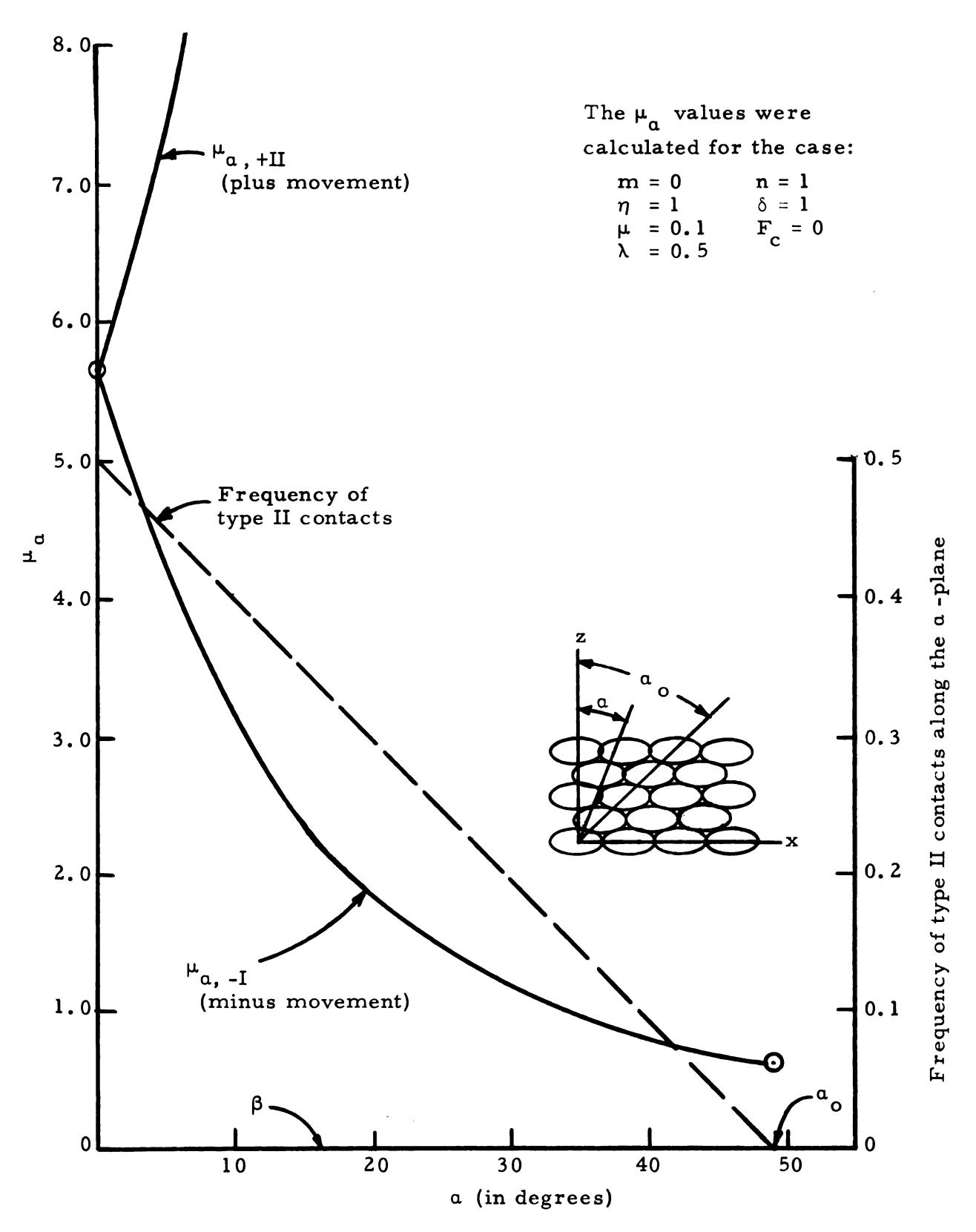


Figure 2.21. The effect of the shearing angle on μ_α and the frequency of type II contacts.

The yield strength for minus movement is a maximum at $\alpha + \beta = \gamma$ and a minimum at $\alpha = 90^{\circ} - \beta$. Thus failure is more likely for α -values near this minimum than in other planes. The effect of some of the other variables can be seen from the equations used in deriving Equation 2.14. These observations are:

- 1. The yield strength is a function of the shearing angle a and $\mu_{\alpha} \geq \mu$.
- 2. As the particles are moved farther apart in the stack, the strength decreases.
- 3. As the particle shape becomes longer and more slender, the strength increases.
- 4. As the internal friction of the material increases, the effect of the shearing angle decreases, that is, the strength at small α -values decreases and the strength at large α -values increases.
- 5. If the void ratio of the stack decreases, the effect of the shearing angle decreases.
- 6. As the cohesion of the material increases, the effect of the shearing angle decreases.

A related topic which should be investigated in future studies is the effect of an internal compressive force (stress) in the body on the yield strength. If this stress acts parallel to the a-surface it should tend to increase the possible tangential force along the a-plane before sliding takes place. Another point which should be studied is the internal force state necessary to prevent the surface particles from rotating when a tangential and normal surface force is applied.

This study was limited to incipient motion (failure). The case of continued motion (plastic flow) should also be studied using the same methods.

2.2. The Continuous Mass Approach

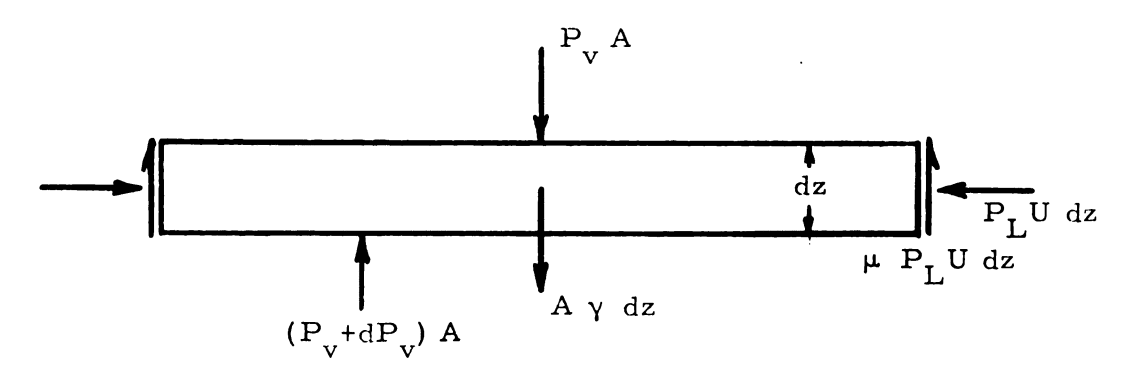
2.2.1. Review of literature

The assumption of a continuous material with the added constraints of isotropy and homogeneity has been used extensively to reduce complex problems to a more easily solvable form. In the area of stresses in grain, the first theoretical study using this assumption was made by Janssen (1895). He considered the element shown in Figure 2.22 and derived formulas for the lateral and vertical pressures exerted by grain in bins. With this force balance and by defining $k = P_L/P_v = constant$, Janssen was able to integrate the derived differential equation to obtain

$$P_{v} = \frac{\gamma R'}{k \mu'} (1 - \exp \frac{-k \mu' h}{R'}),$$
 (2.17)

where R' = A/U, the hydraulic radius and h was the height of the grain. The assumption that k was constant throughout the material has not been supported by experiments; however Janssen's formula is still commonly used and is recommended by Hall (1961) for calculating grain pressures in deep bins.

Terzaghi (1943) considered arching in sand over a yielding trap door. Using the forces acting on the element of material shown in Figure 2.23, and the same procedure as Janssen, he found the vertical pressure on the yielding surface to be



P. - vertical pressure

 P_{τ} - lateral pressure

γ - bulk density of the grain

U - circumference of the bin

 μ^{1} - coefficient of friction of grain on the wall

A - cross sectional area of the bin

Figure 2.22. The force element used by Janssen.

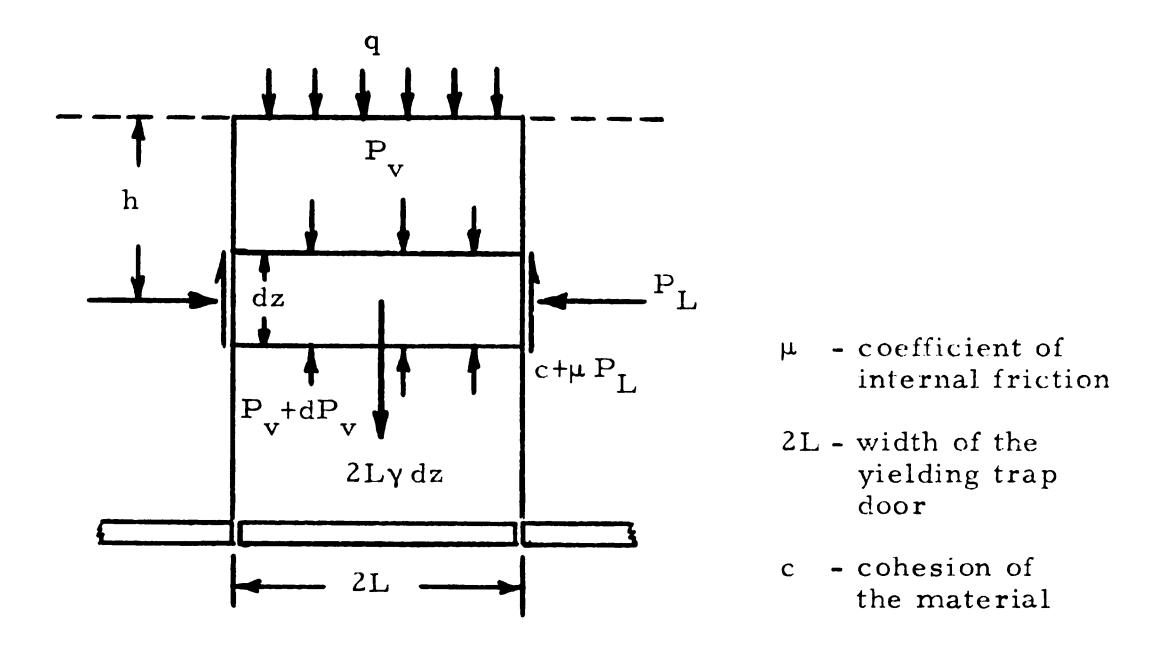


Figure 2.23. The force element used by Terzaghi.

$$P_{v} = \frac{L(\gamma - c/L)}{k \mu} (1 - \exp \frac{(-k \mu h)}{L} + q \exp \frac{(-k \mu h)}{L}$$
 (2.18)

In tests with sand, Terzaghi (1936) found that the stresses in the sand mass above a height equal to two or three slit widths (4L to 6L) were not changed by the yielding of the trap door. Thus the shearing stresses which act on the sides of the element were assumed to be active only in the lower portion of the mass. The upper portion of the mass acted only as a surcharge on this shearing section.

Love (1929) derived the stress distribution equations for a vertical load applied over a rectangular surface area of a semi-infinite elastic material.

Fröhlich (1934) considered the similarity between the vertical pressures in an incompressible, isotropic, elastic material contained in a silo and the same material lying in a semi-infinite space. He derived an expression for the vertical pressure in a silo by taking a semi-infinite space of material and assuming that only the material inside the silo boundary had weight; the portion of the semi-infinite space outside the silo boundary was weightless but could transmit stresses. The equation for the vertical pressure in a semi-infinite space of elastic material with a uniform applied load on part of the boundary had been solved by earlier researchers (Boussinesq). Applying a uniform load on the boundary of the semi-infinite space over a region equal to the silo cross section, Fröhlich found that the vertical pressure at similar points in the two situations would give equal deformation if the applied load had a magnitude of γE , where y was the bulk density and E was the modulus of elasticity of the material.

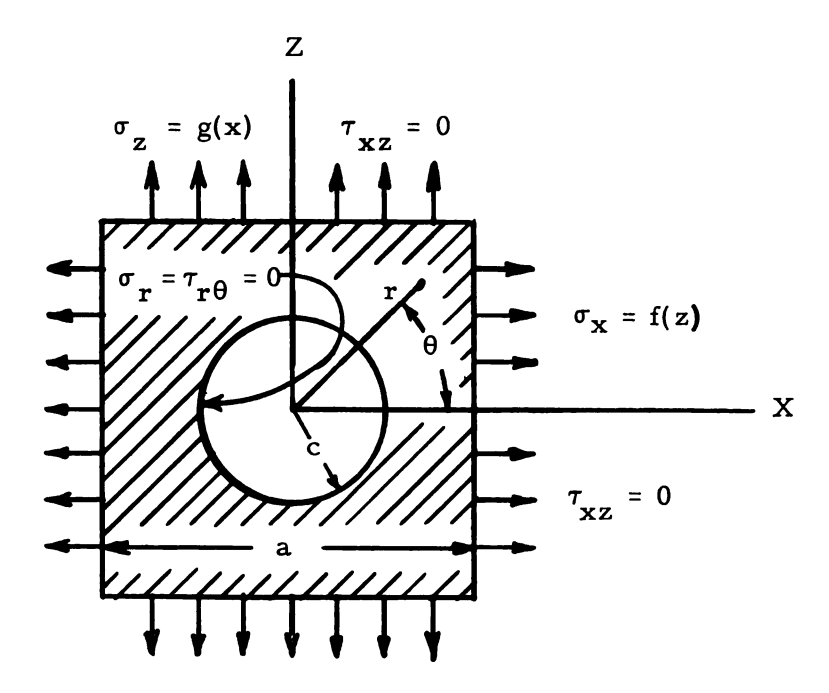


Figure 2.24. A finite square plate with a hole in the center showing the boundary conditions used by Schlack and Little.

The problem of determining the stresses acting in an arched cohesive material is somewhat similar to the elasticity problem of a finite plate with a hole in the center. Solutions to problems of this type, shown in Figure 2.24, were obtained by Schlack and Little (1964) and for a slightly different case by Thompson (1965). This type of approach might give an approximation to the stress field in a shallow bin filled with a cohesive material under a load.

Richmond and Gardner (1962) obtained expressions for the maximum arch span that a cohesive material could form in a vertical channel and the minimum span that could possibly flow under the same conditions. They assumed that:

- 1. the material obeyed Coulomb's failure condition
- 2. the stress was invariant with respect to the vertical coordinate near the free arch surface
- 3. the radial stress component was everywhere equal to the circumferential stress component.

They used differential equations of equilibrium

$$\left(\frac{\partial \sigma}{\partial x} + \frac{\partial \tau}{\partial z} = 0, \frac{\partial \sigma}{\partial z} + \frac{\partial \tau}{\partial x} = \gamma\right)$$

to derive their formulas. Tests with clay agreed closely with the arch spans obtained for the minimum span that could possibly flow. This equation was

$$L = \frac{c}{2v} (1 + \sin \phi)$$
, where $\phi = \text{angle of internal friction.}$

Lenczner (1966) extended this development to non-vertical walls.

Jenike (1962) developed a comprehensive solution to the problem of gravity flow of granular materials based on the theories of plasticity. He assumed that the materials were rigid-plastic, and that in the plastic regions the solids were isotropic, frictional, cohesive and compressible. Jenike and Shield (1959) developed a special yield function for granular materials; this yield surface was a generalization of the commonly used Tresca yield criterion. The yield surface was made a function of the hydrostatic pressure, which changed the hexagonal prism of Tresca into a pyramid. This pyramid was bounded on the pressure side by a flat hexagonal base perpendicular to the axis and the vertex of the pyramid was rounded off. The size of the pyramid was a function of the density of the material, time of

consolidation at rest, the temperature, and the moisture content of the solid. These assumptions were applied to the theories of plasticity and resulted in a series of complex differential equations. Jenike obtained solutions to these equations numerically and displayed these solutions in a series of graphs. He also developed a special direct shear testing machine for evaluating the properties of the solids; the properties measured were the effective angle of friction, the flow functions, the bulk density, and either the static or kinematic angle of friction. This system was used for designing a bin and hopper system with optimum gravity flow characteristics, based on the measured properties of the material.

Many studies have been made to measure the pressures exerted by grain in storage bins. Early experimental work was carried out by Roberts (1883), who concluded that the total vertical force on the bottom of a bin was much less than the total weight of the grain in the bin. He found that the total vertical force on the bottom of the bin did not increase after the height of grain exceeded two bin diameters. The theory of Janssen was checked by many observers. Jamieson (1903) and Lufft (1904) confirmed Janssen's formula by experiments with grain in both model and full sized bins and silos. Ketchum (1919) summarized the work of the research workers of that period (Roberts (1883), Airy (1887), Janssen (1895), Tolz (1897), Bovey (1903), Jamieson (1903), Lufft (1904)). From the work published up to that time, Ketchum concluded that Janssen's assumption of a constant ratio, k, between the lateral and vertical pressures in a bin was not completely true. Data showed that k was not constant but varied

with different grains and different bins and that k increased with the depth of grain.

Several research workers have attempted to measure k for different materials and different bins. Caughey et al. (1951) measured k for wheat, shelled corn, soybeans, sand, pea gravel, and cement, in an 18 inch inside diameter, 5 feet deep, concrete bin. They found that k decreased slightly with depth for wheat and pea gravel, but that k increased with depth for cement and that no relation between depth of material and k was apparent for soybeans, shelled corn, and sand. They concluded from their tests that corn, soybeans, and pea gravel do not follow Janssen's theory, because Janssen's formula gave values of lateral pressure which were larger than their experimental values.

The assumption that a granular mass is isotropic was found to be inaccurate by some researchers. Saul (1953) measured the lateral pressure on the wall and the vertical pressure on the floor of a large bin filled with 10 feet of shelled corn. The bin was filled with corn by three methods and the wall pressures at various depths and the vertical pressures at points along a line across the center of the bin were measured. Saul found that both the lateral and vertical pressure distributions varied considerably with the method of filling the bin. This suggests that the orientation of the grain kernels affected the pressure exerted on the sides and bottom of the bin.

The "dynamic pressures" which act during the filling or emptying of a bin have been found to be much higher than the pressures calculated from Janssen's formula. The magnitude of these pressures was also

influenced by the methods of filling and unloading. This again suggests that kernel orientation affects the pressures acting in a granular mass. This study will not consider moving force systems, however a very good discussion of the research on dynamic pressures can be found in Isaacson (1963) or Turitzin (1963).

Collins and Yin (1965) used motion pictures to analyze the flow patterns in grain. They concluded,

"The observations that raised the most questions were those of the discharge from a central orifice. The gradual orientation of the grains and development of the flow pattern made it clear that no theory could be very useful if it contained the assumption that the grain behaved as an isotropic substance. In particular, if a region of shear failure were predicted by calculation based on this assumption, the actual shear region in the moving grain might be quite different."

2.2.2. Application of the continuous mass approach

Although the experimental evidence from tests with grain seems to make the assumption of a continuous mass somewhat doubtful, these theories have been applied for many years with good results. It is also likely that some agricultural materials such as ground grain, with small granules and some cohesion, might fit the continuous mass assumption quite well. Thus a few of these theories will be used in this study for comparison with experimental results.

The study by Terzaghi (1936) on the pressure in sand over a yielding trap door seemed very similar to the study of arches in grain. Figure 2.25 shows the force system for tests where an arch was formed in a mass of material under a vertical load. In this force system, the assumption was made that the active shearing region was 6L or three slit widths deep and that the portion of the upper section not supported by the side walls acted as a surcharge on the shearing

region. Following the methods of Terzaghi (1943) and assuming c = c' = 0 the vertical pressure acting on the yielding section of the bin floor was found to be:

$$P_{v} = \gamma L(a_3 + a_2b_3) + qb_2b_3 \qquad (2.19)$$

where

$$b_{3} = \exp(-k n_{2} \mu)$$

$$a_{3} = \frac{1}{k \mu} (1 - b_{3})$$

$$b_{2} = \exp(-\frac{2 k n_{1} \mu'}{m_{1}})$$

$$a_{2} = \frac{m_{1}}{2 k \mu'} (1 - b_{2}).$$

At the bottom surface of a stable arch, the vertical pressure P_V must be zero. Using this, along with the assumption that c' = 0, Equation 2.18 was modified to find the cohesion, c, of a material necessary to form a stable arch. The expression for c was

$$c = L\gamma + \frac{L\gamma \ a_2 \ b_3}{a_3} + \frac{q \ b_3 \ b_2}{a_3}$$
.

This solution indicates a maximum arch width for a given material.

The problem of an arched material acting as an elastic body was also considered. A section of such a material with possible boundary conditions is shown in Figure 2.26.

In this solution the arch was assumed to be cylindrical in shape; this allowed the system to be approximated by the plane strain condition. Only the half bin shown in Figure 2.26 needed to be considered because of symmetry. The method of solution follows Schlack and Little; an

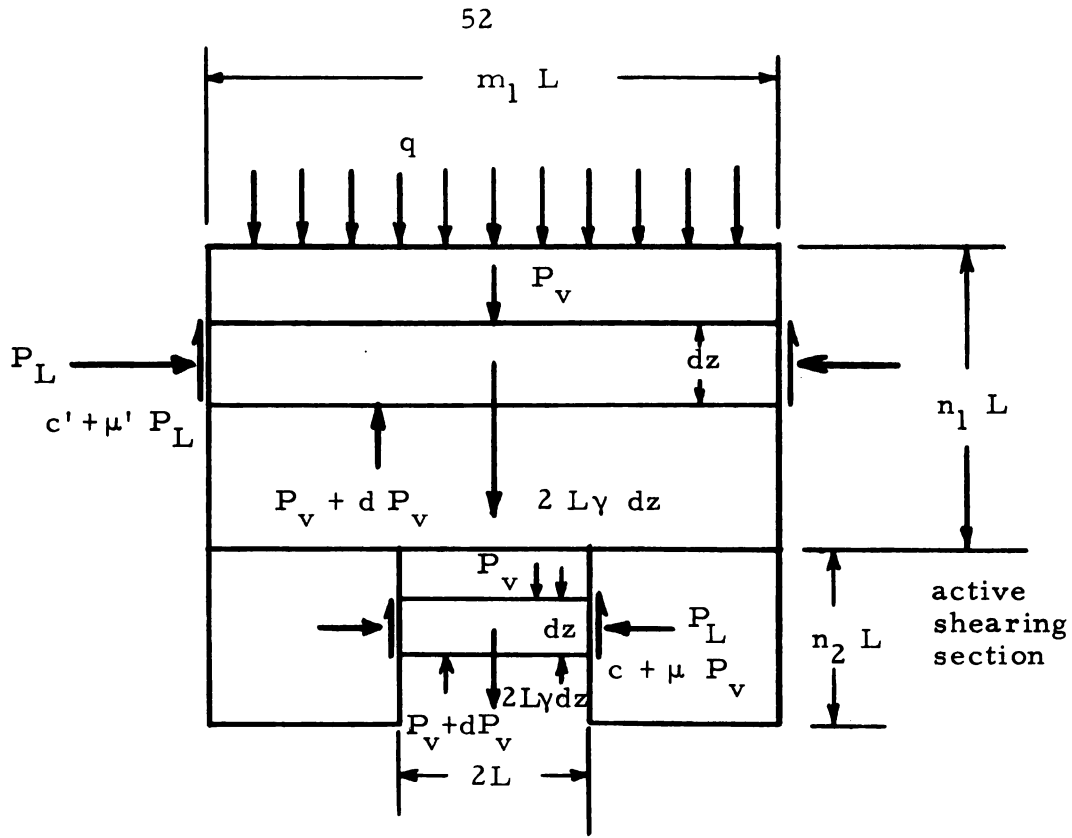


Figure 2.25. The force system in an arched material under an applied vertical load.

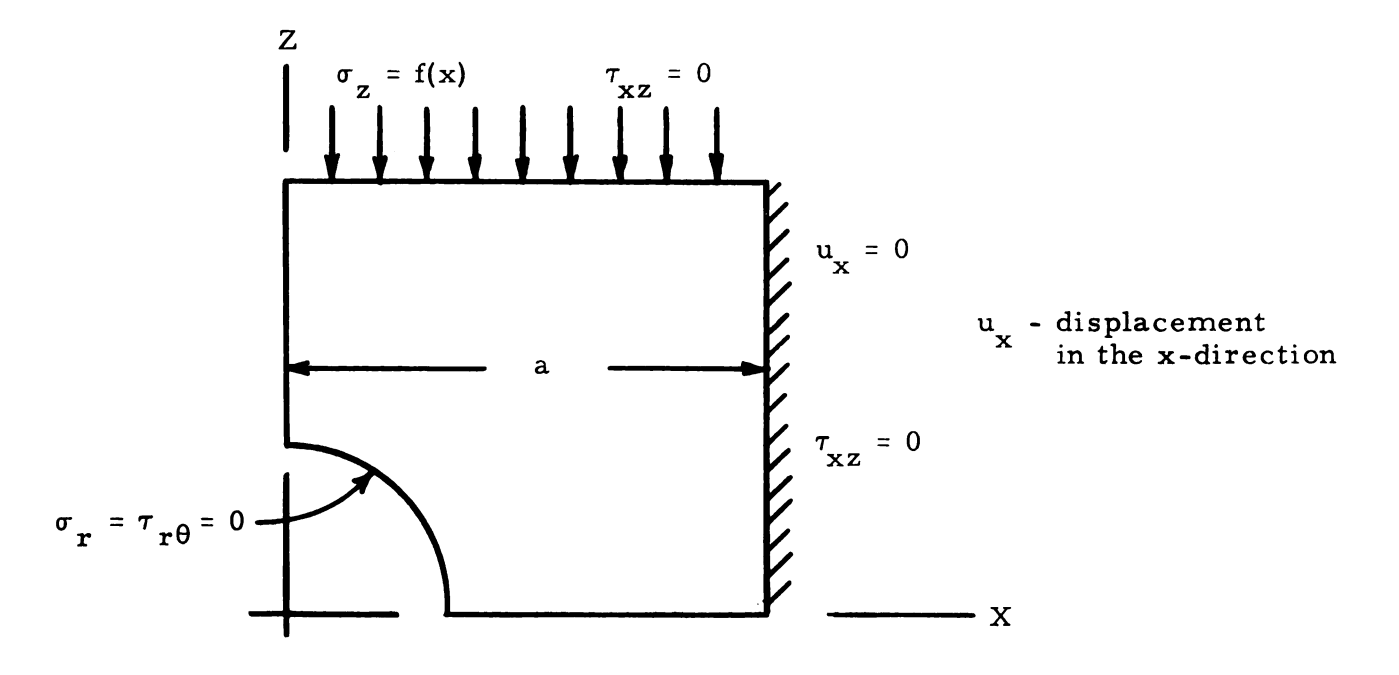


Figure 2.26. An arched material considered as an elastic body.

Airy stress function in the form of an infinite series could be selected so that the conditions on the curved surface are satisfied term by term. Then the boundary conditions on the edges could be satisfied by the method of least squares, that is, by minimizing the specified conditions at a selected number of points on the boundary. This would fix the constant in the truncated stress function and would allow the stress field to be calculated.

The boundary condition of $\tau_{xz} = 0$ at x = a shown in Figure 2.26 does not describe the actual conditions in a bin very well. The actual boundary condition at x = a should be $\tau_{xz} = K \sigma_x$, where K is a constant. It may be possible to satisfy this condition if σ_x is assumed to be the force necessary to prevent movement of the boundary at x = a, i.e., σ_x is the stress on the boundary x = a necessary to maintain $u_x = 0$. Then using the same procedures as above, the boundary conditions of $u_x = 0$ and $\tau_{xz} = K \sigma_x$ may possibly be satisfied.

2.3. The Forces Acting in Particle Arches

2.3.1. Review of literature

Allan (1890) developed the force system acting in a masonry arch by considering a suspended cable; the shape of this cable was determined by the applied load. If this cable was assumed to have rigidity and was inverted, it became an arch. The shape of the cable was also the optimum shape for a masonry arch under similar loading and was defined by Allan as the "line of pressure" of the arch. Under a load which acted uniformly per unit span such as shown in Figure 2.27, this "line of pressure" assumed the form of a parabola.

Figure 2.28 shows an arch under a load with a "horizontal top." With this type of loading, the line of pressure assumed the shape of a catenary.

Roberts (1884), from his tests on the pressures produced by grains in deep bins, concluded that the shape of the grain mass which contributed to the total force acting on the bin floor was parabolic. In studies mentioned earlier, Richmond and Gardner (1962) derived an expression for the shape of the arch formed in a cohesive material; this shape was parabolic. Jenike (1961) arrived at the same conclusion from his more complex study of the same problem.

These results indicated that the shape of an arch might influence its maximum size. Therefore a study was made of the arrangement of particles along arches which were shaped both as parabolas and as catenaries. This study also attempted to determine the force system necessary for the static equilibrium of the particles. Note that the symbols a, L, m, and n as used in this section represent different quantities than in previous sections.

2.3.2. The two-dimensional parabolic arch

The arrangement of particles located along a parabolic arch was studied using the following assumptions:

- 1. The particles are discs of a uniform size (with radius R).
- 2. The center of each particle is located on the characteristic parabola.
- 3. Adjacent particles are in contact.

The arch considered was constructed with relatively few particles.

Figure 2.29 shows the position of the particles if the arch is constructed

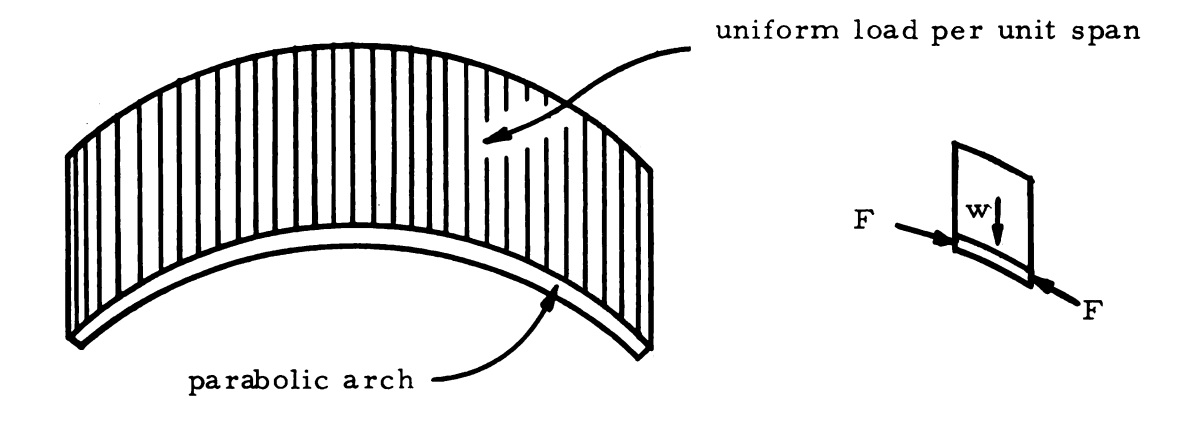


Figure 2.27. An arch under a uniform load per unit span.

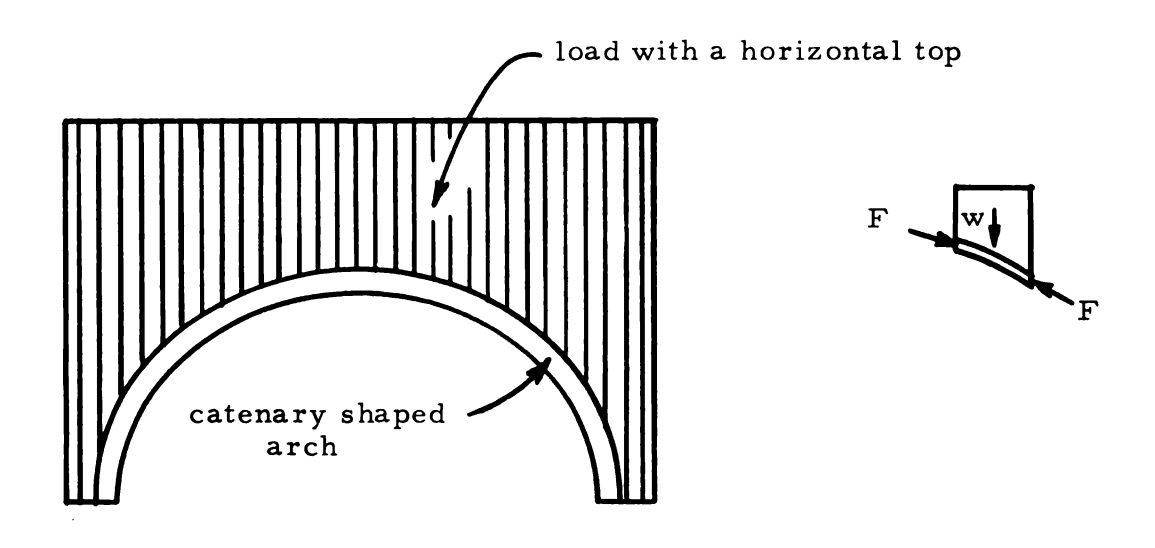


Figure 2.28. An arch under a load with a horizontal top.

of an odd number of particles. The following discussion will treat this case; however, the results will apply to the case of an even number of particles if the coordinates of the center of the first particle are changed. Several of the symbols used in the discussion are defined in Figure 2.29.

The starting condition for the odd-number-of-particles arch was that the center of particle one $(h_1, k_1) = (0, a)$. The center coordinates of any particle (h_i, k_i) must satisfy the equation of the parabola, that is,

$$h_i^2 - 4a^2 + 4ak_i = 0$$
 (2.20)

and

$$h_{i+1}^2 - 4a^2 + 4ak_{i+1} = 0$$

The point of contact (x_i, z_i) of two adjacent particles lies on a straight line connecting the centers; thus

$$x_i = \frac{h_i + h_{i+1}}{2}$$
 and $z_i = \frac{k_i + k_{i+1}}{2}$. (2.21)

Geometry gives

$$(h_i - h_{i+1})^2 + (k_i - k_{i+1})^2 = (2R)^2$$
 (2.22)

Now substituting k_{i+1} from (2.20) into (2.22), gives

$$h_{i+1}^{4} + (8a^{2} + 8ak_{i}) h_{i+1}^{2} - 32a^{2} h_{i} h_{i+1} + A = 0$$
, (2.23)

where

$$A = 16a^{2} (h_{i}^{2} + k_{i}^{2} - 2ak_{i} + a^{2} - 4R^{2}) .$$

The Newton-Raphson formula,

$$F(x) = x - f(x)/f'(x)$$
 (2.24)

was used to obtain a numerical solution for h_{i+1} . For this case, Equation (2.24) becomes

$$F(h_{i+1}) = \frac{3h_{i+1}^4 + h_{i+1}^2 (8a^2 + 8ak_i) - A}{4h_{i+1}^3 + h_{i+1} (16a^2 + 16ak_i) - 32a^2h_i}.$$
 (2.25)

Values for the radius R and the parabola characteristic "a" were assumed and h_{i+1} was found by successive iteration of equation (2.25). The z-coordinate of the center of particle i+1 and the contact point between particles i+1 and i were then calculated from Equations (2.20) and (2.21). A FORTRAN program was written to carry out these calculations.

This same procedure was also used to compute the positions of particles along a catenary, however the results were nearly the same as for the parabola; therefore they were not included here.

2.3.3. Computation of the parabola shape factor "m"

The method outlined above calculated the position of each particle on the parabolic arch for a specified parabola and particle size. However the desired information was the particle position on a parabolic arch when the width of the base of the arch and the number of particles in the arch were specified. To accomplish this the computer program used to calculate the particle position was modified. The steps to carry out this computation are given below:

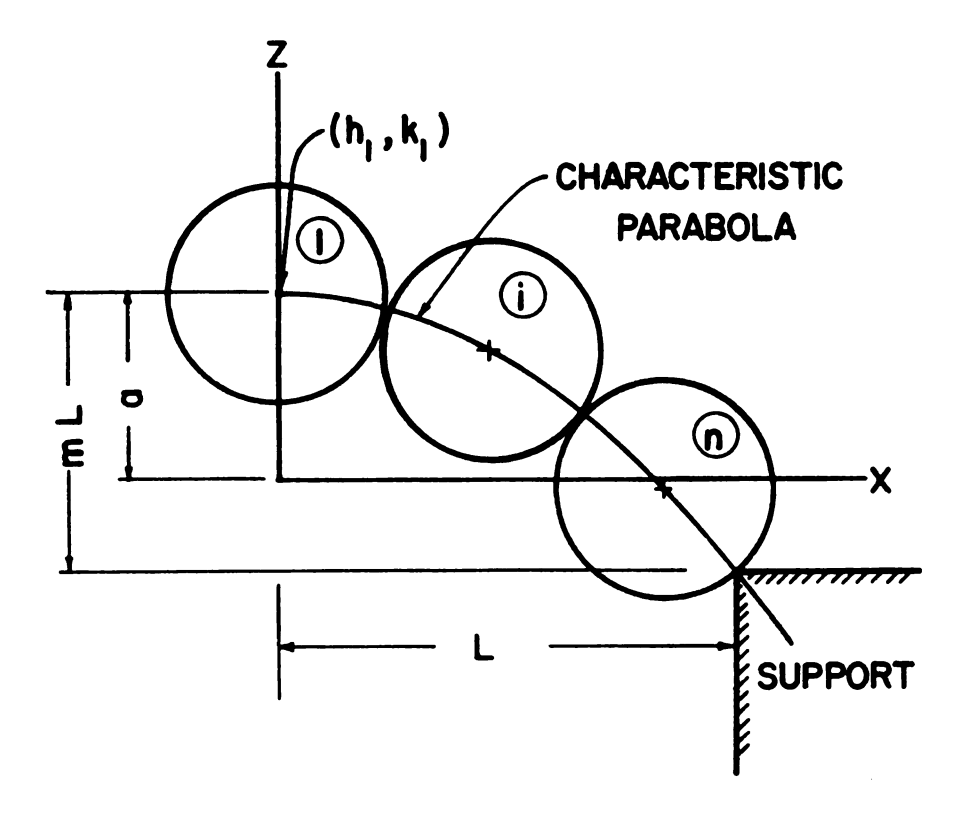


Figure 2.29. A parabolic arch formed with an odd number of particles.

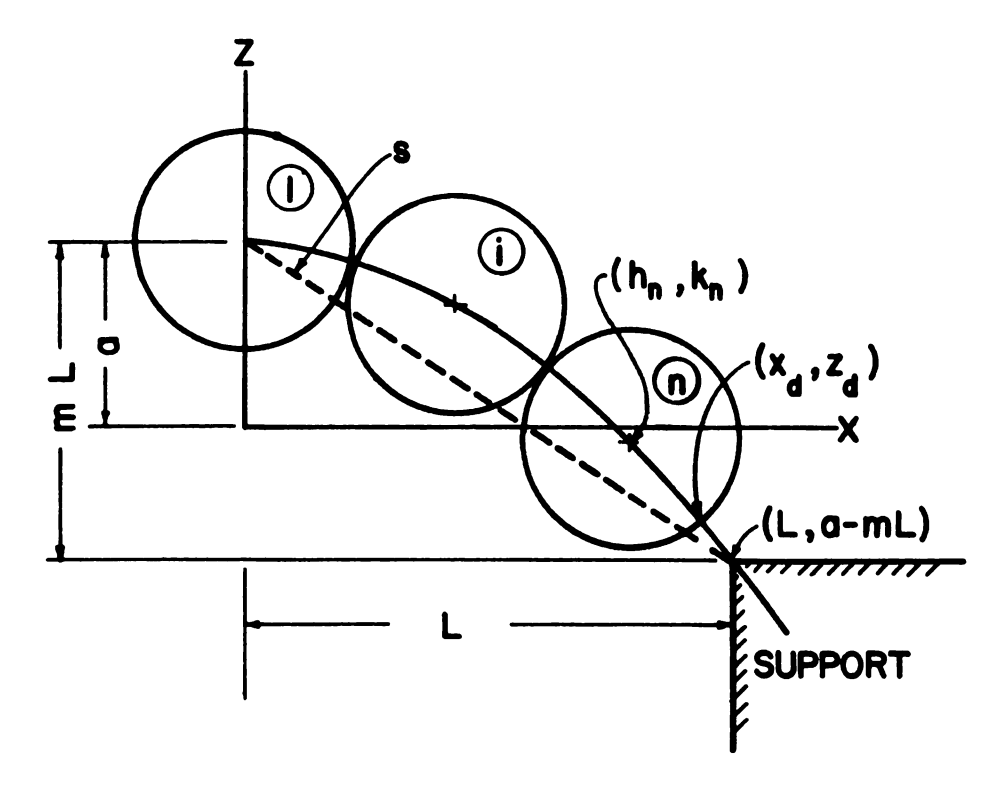


Figure 2.30. The geometry of calculating "m".

1. A first approximation was made for the parabola shape constant m by considering the particle centers as lying on a straight line (see Figure 2.30), thus

$$m = \frac{\sqrt{s^2 - L^2}}{L}$$

where s = NR, and N is the total number of particles in the arch.

2. The parabola characteristic a was chosen so that the parabola would pass through the point (L, a-mL), so

$$a = L/4m$$
.

- 3. The coordinates of all the particles were computed using the methods of Section 2.3.2 using estimated values of a and m. This gave estimated values for (h_n, k_n) .
- 4. The x-coordinate, x_d , of the intersection of the parabola and the particle n was computed. This point should have the value L. If, however x_d was not sufficiently close to L, then m was corrected by the equation

$$m_1 = m \times_d / L$$

and the computations repeated from Step 2 until (x_d-L) was sufficiently small. Thus m was found as a function of L/R and N.

2.3.4. Forces acting in an arch

The force system acting on the particles along an arch was calculated using the following assumptions.

1. The arch was symmetric with respect to the yz-plane.

- 2. The external force on the uppermost particle acted downward.
- 3. The external forces on all particles except the top particle (F_2, F_3, F_4) acted at an angle ϕ_2 to the vertical.
- 4. The friction coefficients acting at all points were equal.
- 5. The moments acting on the particles were zero, so the sum of the friction forces on each particle had to be zero. This implied that the magnitude of the reaction force on the particle was greater than the sum of the magnitudes of the other forces acting on the particle. Thus $F_R \ge F_{12} + F_2$, in the case of the three particle arch.

These assumptions lead to the force system shown in Figure 2.31 for the three particle case.

From this force system, the following equations were derived:

$$F_{12} = (F_1 + w)/(2 \sin \phi_{12} + 2 \mu \cos \phi_{12})$$
 (2.26)

$$F_{2} = \frac{\left[-w\cos\phi_{23} + F_{12}\left\{\sin(\phi_{23} - \phi_{12}) - \mu\cos(\phi_{12} - \phi_{23}) - \mu\right\}\right]}{\left[\mu\sin(\phi_{23} - \phi_{2}) + \cos(\phi_{23} - \phi_{2}) + \mu\right]}$$
(2.27)

$$F_{R} = [F_{12} (\cos \phi_{12} - \mu \sin \phi_{12} - \mu \sin \phi_{23}) - F_{2} (\sin \phi_{2} + \mu \cos \phi_{2} + \mu \sin \phi_{23})] / \cos \phi_{23}$$

$$(2.28)$$

The same type of analysis was carried out for four and five particle arches. The computer program written for Section 2.3.3 was expanded to compute these forces.

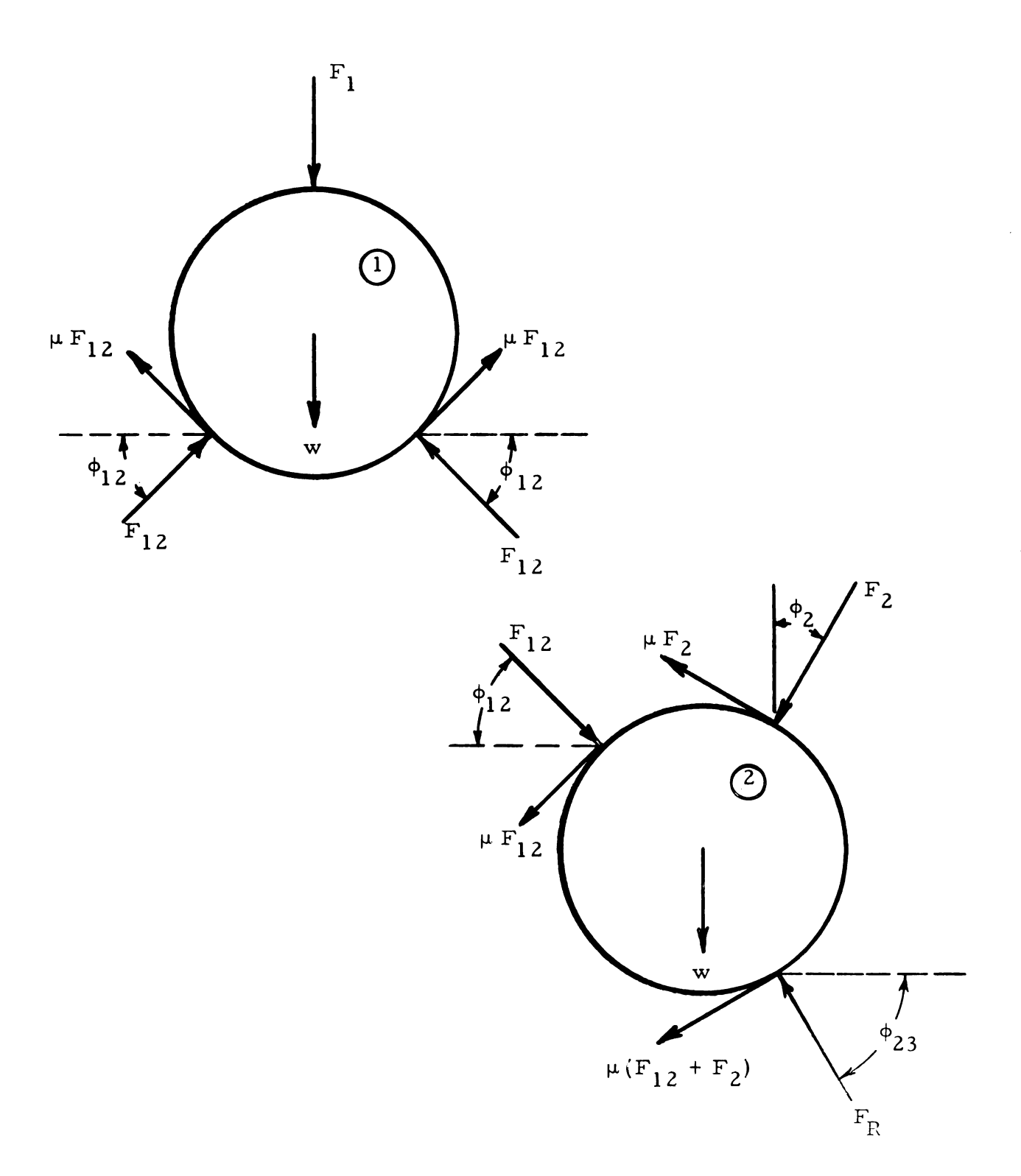


Figure 2.31. The force system acting on particles in an arch.

A force system was considered to be unstable if any force acted in tension, if an external force (F_2, F_3, F_4) necessary for equilibrium was one order of magnitude larger than the applied force F_1 , or if assumption five was not satisfied.

The three particle arches were found to be stable for friction coefficients between - 0.2 and 0.1 and assumption five was satisfied for at least one value of the friction coefficient for all values of ϕ_2 tested. Figure 2.32 shows the relationship between F_2/F_1 and the friction coefficient for two values of L/R. (The ratio L/R will be designated in Section 3.4 by the symbol M.)

The four particle arches were unstable in all conditions; assumption five was not satisfied for any situation tested.

With $\phi_2 = 30^{\circ}$ and with friction coefficients of 0.0 and 0.1, the five particle arches were stable for most L/R values. However as ϕ_2 increased, the force system became unstable. Figure 2.33 shows the relationship between F_2/F_1 , F_3/F_1 and the friction coefficient for two values of L/R.

Even though this part of the study was not carried to a point where conclusions about the stability of arches could be drawn, it might be used as a starting point for future studies. It could be modified by assuming that only every other particle center is on the arch line and that the intermediate particles are some distance behind on a parallel arch, similar to the approach used in Section 2.1. This model would correspond more closely to a real arch.

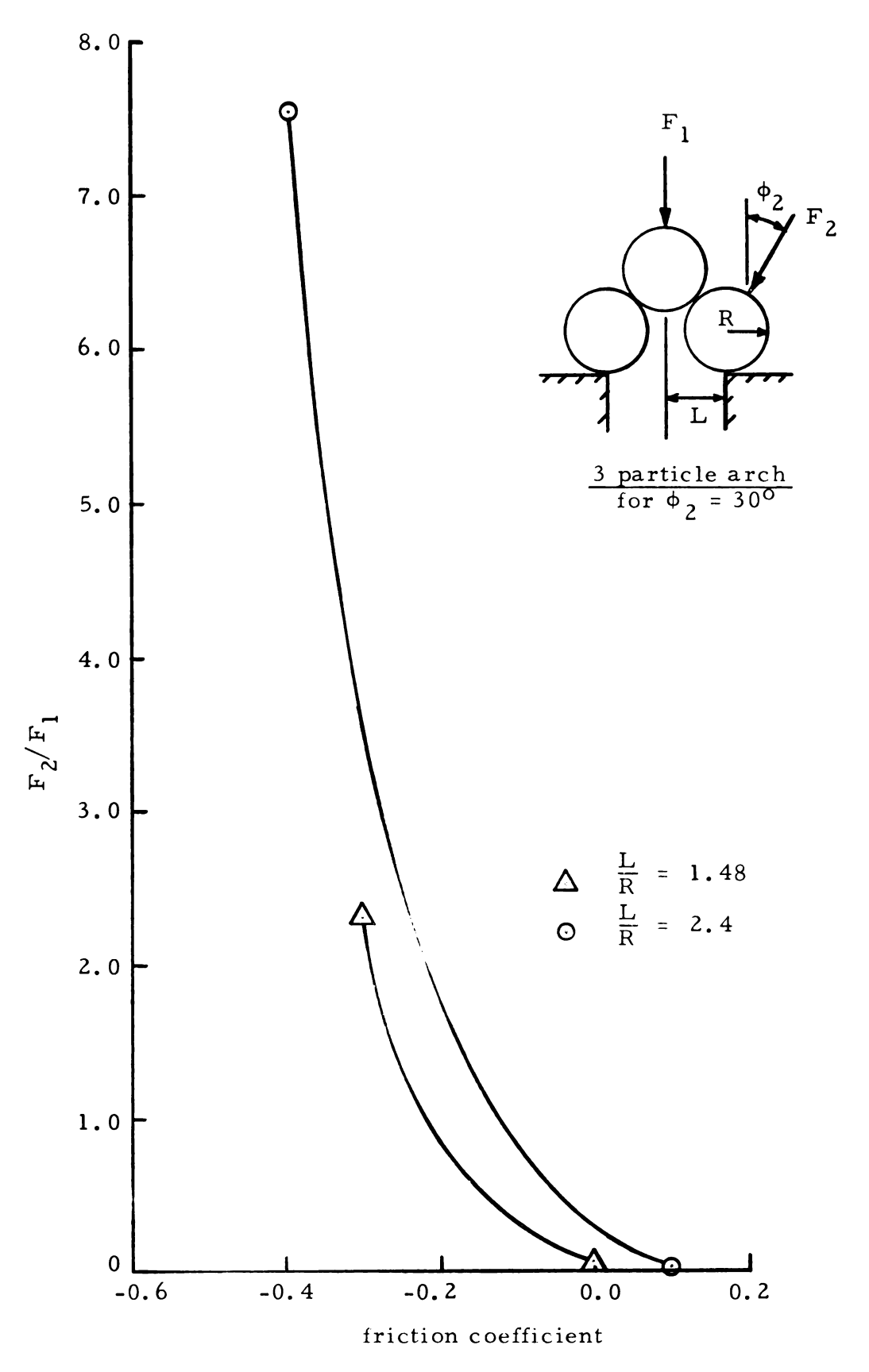
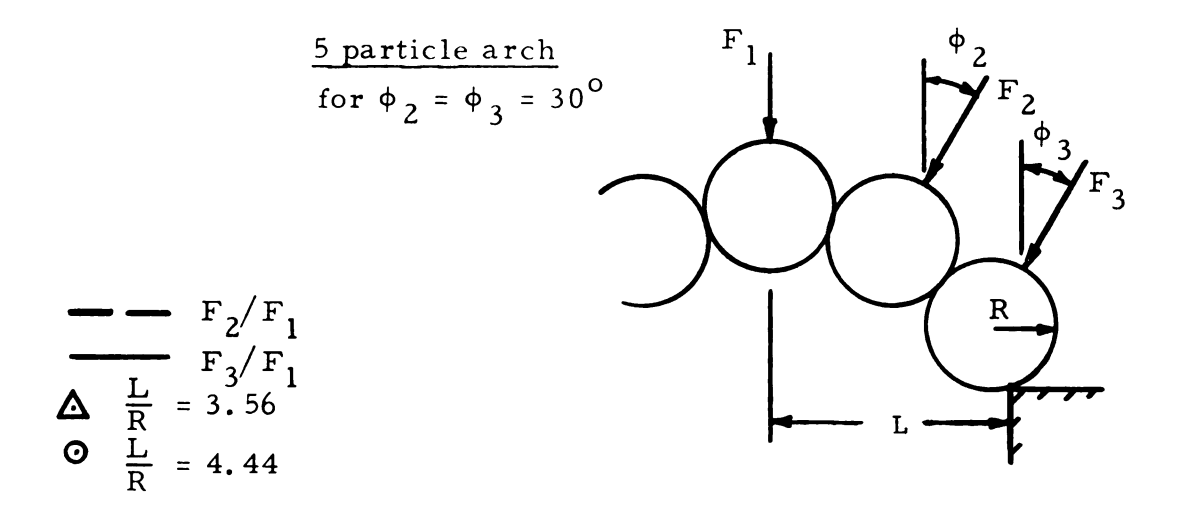


Figure 2.32. The external forces acting on a three particle arch in equilibrium.



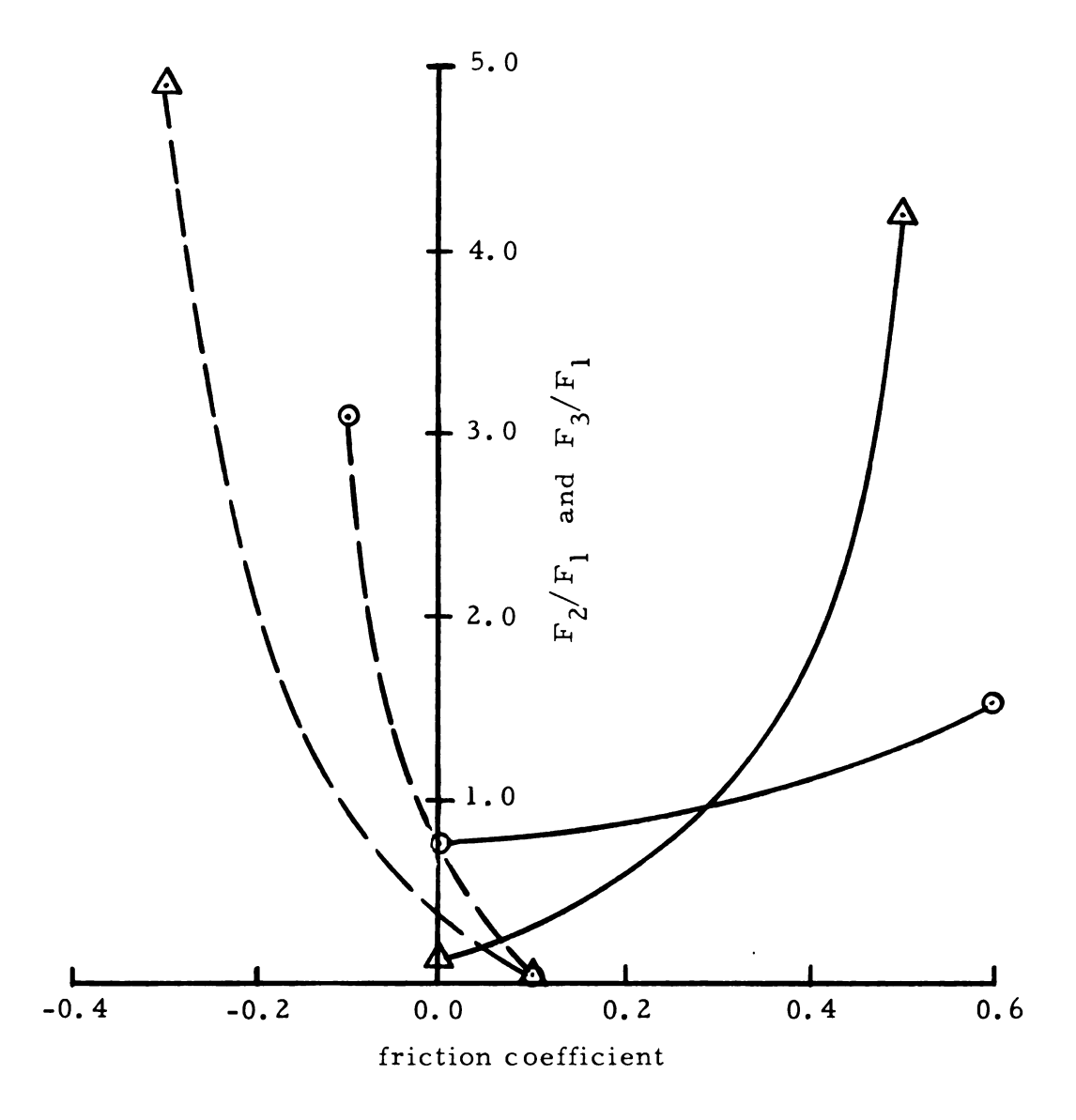


Figure 2.33. The external forces acting on a five particle arch in equilibrium.

III. THE FACTORIAL STUDY

3.1. The Testing System

3.1.1. Apparatus

The model bin used in this study is shown in Figure 3.1. The front and back of the bin were made of Plexiglas so the orientation of the seeds could be observed during the formation of arches. The sides of the bin were made of plywood and could be shifted to permit sloping sides in the bin as well as the flat bottom shown in Figure 3.1. The bottom of the bin was made of two pieces of plywood. The space between these pieces could be adjusted by moving either or both pieces. This space formed the slit through which the test materials flowed and over which the arch systems formed. The bottom pieces were cut on a 45° bevel along the slit. This increased the visibility of the arch through the slit and also insured that the plug, similarly beveled, would fit closely into place and form a smooth bottom in the bin.

For the tests using an applied load, a soft synthetic sponge was placed on top the mass of seeds to distribute the applied load evenly over the surface area. A board was placed on the sponge and lead and steel bricks were used as weights.

3.1.2. Test procedures

The temperature was controlled at 70° F and the relative humidity was maintained between 50% and 60% during the tests, except where otherwise stated.

Before every test, all the seeds were removed from the bin; that was to prevent the seeds reposed on the bin floor from affecting

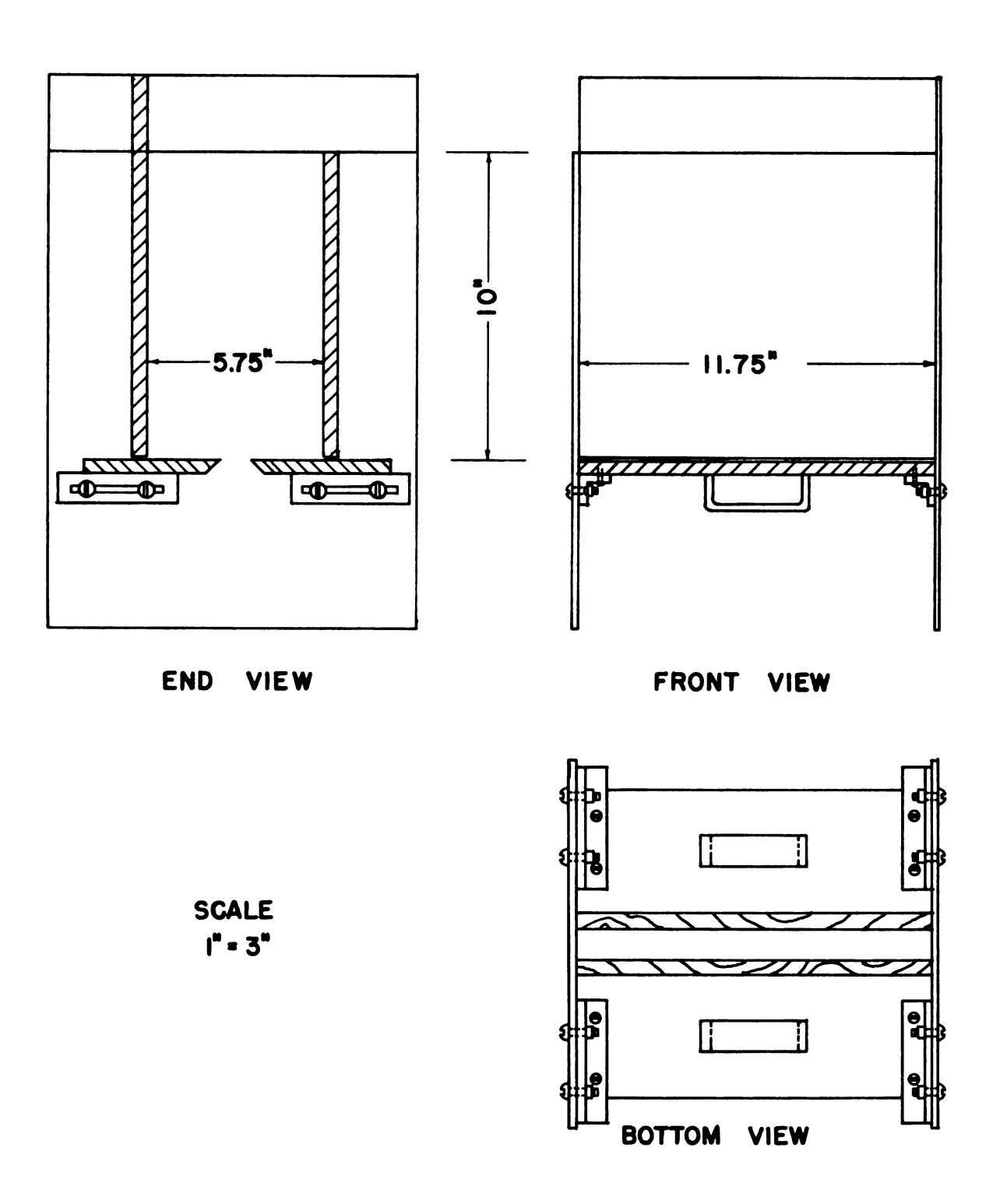


Figure 3.1. The model bin used in the tests.

the orientation of the seeds which were poured in for the next test.

The seeds were compacted by shaking the bin vigorously for ten seconds after each two inch increment of seeds had been added to the bin. The direction of shaking was parallel to the slit length. For all tests, the plug was removed as quickly and gently as possible.

3.1.3. Materials used in the tests

Some information about the materials used in the tests is shown in Table 3.1, and a picture of a sample of each material was shown in Figure 1.1. The pea beans and oats were screened carefully on a

Table 3.1. Particle information

Material	Inform	nation	Bulk density (lb/ft^3)	
	Variety	Mean size (in.) a x b		Compacted
Pea bean	unknown	0.32×0.25	52.0	55.0
Oats	unknown	0.43×0.10	33.6	36.5
Sugar beets	U.S. 215 x 216 raw seed	0.172	18.7	21.0

Clipper laboratory seed cleaner; the mean size was assumed to be the average of the two screens used. The beans passed through a number 17 screen (0.266 in. dia. holes) and stayed on a number 15 screen (0.235 in. dia. holes). The oats passed through a slot screen with 0.109 x 0.75 inch slots and stayed on a screen with 0.094 x 0.75 inch slots. This determined the short dimension of the seeds; the long dimension of the beans and oats was found by measuring a sample of individual seeds.

A sample of sugar beet seeds was taken with a Boerner sampler (see Hall (1957), p. 92). This sample was screened manually and each size division weighed; the weighted average of the size divisions was considered to be the mean diameter of the seeds.

Approximately one-half bushel of each material was used for the tests. During the tests some beans tended to crack and split; these damaged beans were removed by inspection.

3.2. Observations of Arch Systems

Sections 1.2.1 to 1.2.3 contain some introductory statements about arch systems. Included in these sections were definitions of several terms used in the following discussion, photographs of typical arch system in the test materials and a brief description of the arch formations in the test materials.

3.2.1. Orientation of particles

As was stated earlier, beans tended to form flow arches while oats formed mainly initial arches. These characteristics could be partly explained by the shape of the seeds and by their orientation in an arch.

The critical dimension of a bean in forming arches seemed to be its short diameter. The best arch forming position for the individual bean was with the long axis parallel to the slit, however a good arching position was any position with the short axis perpendicular to the slit. For forming arches in oats, the critical dimension seemed to be the length of the kernel. Therefore the oat kernel formed arches best if its long axis was parallel to the bottom of the bin and perpendicular to the slit.

When particles flowed, their long axes tended to line up with the flow lines which formed in the material. These flow lines radiated up and out from the slit in a hyperbolic shape. Thus when beans were flowing, their axes were positioned in a good position for arching while the oat kernel was placed in an unlikely arching position during flow.

Compacting these materials before opening the outlet tended to position them with their long axes parallel to the bin bottom and perpendicular to the slit. Tests showed that the arching properties of beans were not affected by compacting, but that the arch span of an oat arch was increased by compacting.

Beet seed did not have any prominent axial symmetry, so no conclusions about its arching properties could be drawn from particle orientation.

3.2.2. Primary-secondary arch systems

These types of arch systems were defined in Section 1.2.2 and photographs of actual arch systems were shown in Section 1.2.3.

In a stable arch condition, primary arches normally occurred about four to eight particle diameters apart along the length of the slit. However occasionally several primary arches formed adjacent to one another, resulting in a stronger arch system. Usually only three to five particles made up a primary arch in beans; thus the arch was strong in the vertical direction but weak in the lateral direction. Certain particle arrangements in primary arches appeared frequently; they were classified into three divisions:

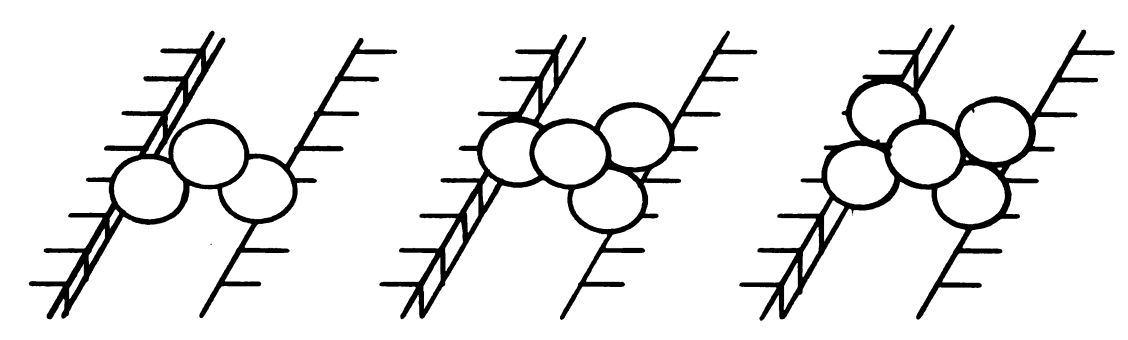
- a. type l, linear
- b. type 2, delta based
- c. type 3, square based

Sketches of these three types of arches are shown in Figure 3.2.

These arches were idealized; an actual arch system had many variations due to the random arrangement of the particles in the material. From observing many arch systems, the delta-based arch seemed to occur

more often than the others.

A series of tests was made to determine the effect of primary arches. A group of narrow (less than one particle diameter) sheet metal strips was laid across the slit at regular intervals to simulate primary arches. After the strips were in place, the bin was filled with beans, the slit opened and flow observed. If flow stopped at any time during the outflow of approximately ten inches depth of beans which was used in each trial, a stable arch system was considered to have formed. The results of the tests with beans are shown in Table 3.2.



Type 1, linear Type 2, delta based Type 3, square based

Figure 3.2. Types of primary arches.

Table 3.2. Percent of trials in which stable arch systems formed in beans for various slit widths and strip spacings.

Width of slit	Strip spacing in particle diameters*						
(part. dia.*)	47	15.2	7.2	6.0	5,2	4.6	4.0
1.75	100%	100%					
1.9	10	40	100%				
2.0	0	0	30	80%			
2.13	0	0	0	10	40%	100%	
2.25	0	0	0	0	0	30	100%
2.4	0	0	0	0	0	0	0

As can be seen from Table 3.2, the strips did cause stable arches to form over wider slits. However, from observing arches formed over slits, it appeared the strips were not as effective in forming arch systems as granular primary arches because the strips did not provide the same support for adjacent arches as did the granular arches.

Tests with strips in sugar beet seed increased the width of the arched systems in loosely poured granules; however, the same widths were obtained without strips in compacted seed. Using the strips with oat kernels had very little effect on the width of slit over which a stable arch system would form.

Secondary arches were formed by five to ten particles, were four to eight particle diameters in length and extended up to four particle diameters into the grain mass. Secondary arches were much more prominent in systems formed with nearly spherically shaped particles

^{*} Particle diameter was assumed to be 0.25 inches.

such as beans than with cylindrically shaped particles such as oats.

Because of their size, it would seem that the secondary arches would be very unstable in the lateral direction and would also contain particles which are difficult to support in the vertical direction. However the arch system over a slit was constructed similar to a vaulted ceiling along a corridor with supporting cross arches (primary arches) at regular intervals, so the secondary arches received both vertical and lateral support from the primary arches and adjacent secondary arches.

Secondary arches were much more variable in shape, size and construction than were primary arches.

3.2.3. Other observations

Preliminary tests were made using a plug for the slit which did not fit into position exactly. After a few tests, a properly fitting plug was made and a change in the formation of arches was noted. Further experimentation showed that if the plug was slightly below the bottom of the bin, stable arch systems formed more readily than with a properly fitting plug. But if the plug was very loose (about one-half particle diameter below the bottom of the bin), stable arch systems did not form as often as with a properly fitting plug. This was probably due to the positioning of the particles into favorable arching positions in the first case and into unfavorable positions in the second case.

A second construction error pointed out another factor which influenced arch formation. During the building of the bin a small gap was left between the bottom of the side walls and the moveable bottom.

This gap was originally large enough to permit some particles to fall

out. After reducing this gap a noticeable increase in the frequency of stable arch systems was found. This is possibly the same effect as was mentioned by Lee (1963) in his discussion of the "expanded outlet" method of promoting flow.

3.3. Factors Influencing Arching

After these initial observations, a more systematic study of the factors influencing the arching of the test materials was outlined and partly executed. The factors selected as having the most influence upon the arching of a material were assumed to be:

A. Particle properties

- 1. size
- 2. shape
- 3. density
- 4. friction
- 5. elastic properties
- 6. adhesion
- 7. cohesion

B. Stacking characteristics

- 1. particle orientation
 - a. in flow and initial arches
 - b. as a result of flow
 - c. due to bin shape
 - 1) slope of walls
 - 2) flat bottomed
 - 3) bin outlet size and shape

2. load on particles

- a. at the time of arch formation
- b. previous loading history

Only some of these factors were studied systematically; the results are reported in Sections 3.4, 3.5 and 3.6.

3.4. Gap Width-Particle Size Relationship

3.4.1. Review of literature

The ratio M of width of opening to the mean particle diameter has been used by several authors to describe the smallest opening through which a material will flow. Aytaman (1959) investigated the "hanging" of dry granular sandstone in vertical pipes. He found that flow from a pipe depended on the ratio M. Based on his tests the flow results were:

free flow range $4.21 \le M$ probable flow range $2.24 \le M \le 4.21$ no flow $M \le 2.24$

In the probable flow range Aytaman determined a critical height of material in the pipes which was necessary to cause "hanging". If a pipe was filled with sand below this critical height, no hanging would occur, but if sand was filled above this critical depth, hanging did occur.

Brown and Richards (1959) listed values for M for several materials; these values are given in Table 3.3. They found the ratio M for circular orifices to be approximately twice the M value for flow through narrow slits.

In the discussion following Brown and Richards' paper, Fowler reported "bridging" and erratic flow at an M of between four and six.

Langmaid and Rose (1957) measured the minimum opening size for flow of ground and forged steel balls, flint gravel, and sheet iron punchings (9/64 by 6/64 and 8/64 by 4/64, all dimensions in inches) and found that M was nearly equal for these materials. The values they found were M = 2.68 for slits and M = 4.32 for circular apertures.

Because the flow became erratic and flow stoppages occurred randomly as the aperture became smaller, direct measurement of this dimension was very difficult. In a further study Brown and Richards (1960) noted that very few particles flowed through a region near the edges of an aperture. They measured the flow rate for their test materials through several sizes of circular and rectangular openings. They plotted the dimension of the opening against the characteristic length

$$\left[\frac{Q}{\ell \rho \sqrt{g}}\right]^{2/3},$$

where Q was the flow rate, ℓ was the slit length, ρ was the density of the material, and g was the acceleration of gravity. This plot formed nearly a straight line which Brown and Richards extended to the zero flow point. This intercept point they termed the "d_k" of the material; the "empty annulus" or small region around the edge of an opening through which very little material flowed was equal to $d_k/2$. The d_k value was nearly equal for both circular and rectangular

apertures. In other tests they found that the smallest size of slit through which a material could be induced to flow by tapping agreed with the predicted d_k , however the minimum size of circular opening through which a material would flow was two to three times d_k . Brown and Richards correlated their flow data to an effective aperture size which was the apparent size minus the empty annulus. Other authors have defined this effective aperture as $(D-C_2\overline{d})$, where D is the actual aperture size, C_2 is a material constant, and \overline{d} is the mean particle size. This value was calculated from the data given by Brown and Richards and listed with their original data for comparison.

Table 3.3. Flow properties of several materials (Brown and Richards)

Material	mean size \overline{d} (cm)	M-value (circular orifice)	^d k (cm)	С2
Large beads	0.101		0.13	1.29
Small beads	0.025	4.1	0.041	1.64
Sand	0.059		0.10	1.7
Tapioca	0.168		0.22	1.31
Sand Yl	0.074	4.3	0.12	1.62
Sand Y2	0.051	4.6	0.079	1.55
Sand Y3	0.025	5.6	0.036	1.44
Coal	0.098	7.0	0.14	1.43

Welschof (1960) carried out much the same procedure with wheat. He plotted the opening size against the characteristic length

$$\left(\frac{Q}{\rho'\sqrt{g}}\right)^{2/5}$$
,

where Q was the flow rate, g was the acceleration of gravity, and

 ρ ' was the "flow density" of the material. Welschof found d_k for wheat (\overline{d} = 0.391 cm) to be 0.6 cm or C_2 to be 1.53. The minimum orifice diameter for flow of wheat was found to be 1.5 cm, giving an M value of 4.

Beverloo, et al. (1961) also considered a region of no flow around the edge of an orifice in a flat bottomed cylindrical container. They defined the effective orifice diameter as (D - C_2 \overline{d}) and calculated C_2 for several materials from their flow data. Table 3.4 gives their results. With the exception of sand, their results agree closely with the data of Brown-Richards.

Table 3.4. Orifice reduction constant for several small seeds (Beverloo, et al.)

Material	Mean size \overline{d} (cm)	C ₂	Material	Mean size \overline{d} (cm)	C ₂
Sand	0.045	2.9	Rapeseed	0.17	1.4
Linseed	0.25	1.5	Kale	0.18	1.4
S pinach	0.30	1.4	Swede	0.18	1.4
Watercress	0.16	1.3	Turnip	0.17	1.4

Several other researchers, Deming and Mehring (1929), Rausch (1948), Rose and Tanaka (1959), have conducted studies of the flow of granular materials from conical outlets. Their data agreed in general with the values quoted above.

3.4.2. Results of tests

The tests made in this study measured the maximum slit over which an arch would form, whereas the data reported above measured the smallest opening through which a material would flow. These two dimensions should be quite similar, however, for non-cohesive

materials. Table 3.5 gives the M-values measured in this study.

Table 3.5. Maximum arch widths for test materials

Material	M-value - over a slit (based on large particle dimension)	M-value - over a slit (based on small particle dimension)
Bean	1.5	1.9
Beet seed - loose	3.0	3.0
Beet seed - compacted	6.0	6.0
Oats - loose	1.2	5.3
Oats - compacted	1.4	6.0

These M-values were for flow through a narrow slit and must be doubled for comparison with the values in Table 3.3, which were measured for flow through a circular orifice. Considering this, the values measured here are generally similar to the previous measurements, but they show a wider range because the variability of the particle characteristics was greater in this study than in the other studies.

3.4.3. Comparison with the results of Section 2.3.4

The assumptions made in the analysis of Section 2.3.4 limited the value of the calculated results. Assumption three excluded the possibility of only one or two of the friction forces acting in the opposite direction to those shown in Figure 2.31. However, if this assumption was not made, many combinations of force systems would be generated. This assumption also was the basis for assumption five.

The arches with all of the particles in one plane used in the analysis were not often observed in real arch systems. Instead the

arch would normally have two supporting particles at either or both ends (see Figure 3.2). However the theoretical results could be extended to the non-plane case by using an apparent radius R' based on the contact points between the particles.

Real primary arches in beans, the test material most nearly fitting the assumptions of the theory of Section 2.3.4, were very short, usually less than a three-particles-in-a-plane arch in length. The theoretical analysis showed the best stability for the three particle arch. The five particle system was found to be stable under some conditions, but no five particle arches were found in the tests.

One reason why five particle arches did not form in beans was the low probability that five particles would be in the proper position to form an arch. Because these tests were made over a long slit, flow stopped only if several primary arches formed at nearly the same instant, reducing the probability of a stable arch system even more.

Another reason for the destruction of five particle arches might have been an unbalance of forces in the y-direction. An assumption inherent in the linear arch system was that the lateral forces were in equilibrium. The formation of a five particle arch was probably affected more by lateral instability than the formation of a three particle arch.

3.5. Effect of Applying a Vertical Load to the Grain Mass

It seemed very likely that the stress state in the grain mass should influence the formation of arches. For an initial arch, the static stress conditions would apply. Therefore some studies of these conditions were included.

3.5.1. Review of literature

Kramer (1944) measured the ratio of lateral to vertical pressure, k, in a bin of rough rice 2 ft deep and 1 ft square. He used 4 in. square pressure sensors to measure the pressure on the wall and floor of the bin. He found that k increased from 0.3 to 0.47 as the vertical pressure increased from 100 psf to 500 psf. Kramer also noted that only 27% of the applied load was transmitted to the bottom of the bin. In tests on small grains, Lorenzen (1957) measured the ratio k in a "pressure resolution chamber". He believed that the best method of determining k was with a triaxial compression chamber, but the "pressure resolution chamber," which measured the stresses in all three dimensions was easier to use than a triaxial compression chamber. For applied vertical pressure of 1 to 11 psi, Lorenzen found that k varied with the applied pressure, especially for vertical pressures below 3 psi. The variation depended upon the grain, increasing with some grains and decreasing with others.

In tests with commercial white sand Aytaman (1959) studied the arching of sand under high pressures. He found the pressure needed to cause arching depended on M. He observed that the effect of pressure on the sand in the pipes seemed to be confined to the 2 or 3 in. directly below the piston applying the pressure. The shape of the arches

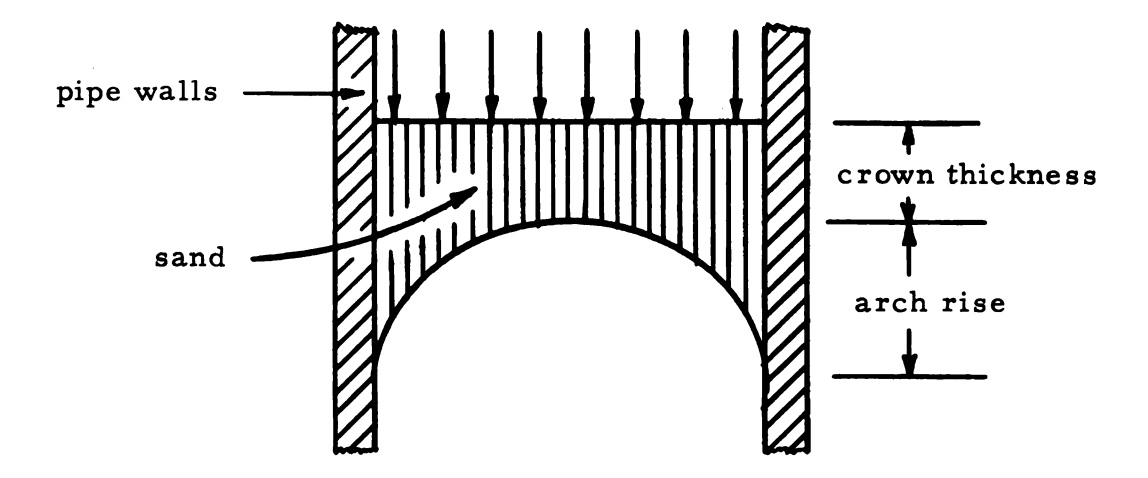


Figure 3.3. Arch shape factors measured by Aytaman.

was measured (see Figure 3.3); the rise of the dome decreased as the pressure increased and for a given pipe size the arch rise increased as the particle size decreased. Crown thickness also increased as pressure increased. The pipe was initially filled with sand.

LaForge (1962) measured the flow rate of several materials through orifices in the sides and bottoms of cylindrical, flat bottomed bins. During tests in an 8 in. diameter bin with a 1.25 in. circular orifice in the bottom, he found a slight decrease in the flow rate of plastic globules ($\overline{d}=0.0226$ in., $\gamma=53.4$ lb/ft³) as the pressure applied to the surface of the globules increased from 0 to 4 psi. The flow rate remained nearly constant for pressures from 4 to 7 psi. The flow tests were terminated when about eight in. of globules remained in the bin. Other tests with wooden beads ($\overline{d}=0.390$ in., $\gamma=25.8$ lb/ft³) through a 1.75 in. orifice in the same bin were unsuccessful as the beads stopped flowing before the tests were finished whenever any pressure was applied.

Simons and Hare (1965) attempted to measure the elastic modulus of grain in an 8 in. diameter cylinder, 54 inches long, by applying pressure to the top of the grain column. They found that applying pressure increased the lateral pressure much more at the top of the grain column than at the bottom. A Teflon lining was applied to the cylinder walls to reduce friction and the load transmitted to the bottom of the cylinder increased from 28% to 45.6% of the top load which was still not suitable for obtaining accurate data. Simons and Hare then changed to a 1 in. deep grain column and measured the stress strain relationship for shelled corn at several moisture contents. They found that the sample had to be vibrated a minimum of 90 seconds to give reproducible results over the pressure range of 2 to 30 psi which they used.

Narayan and Bilanski (1966) used 5 in. deep grain samples in cylinders with 4 in., 6 in. and 8 in. nominal diameters to measure the elastic properties of wheat. They applied pressures over the range of 125 to 3000 psi, measured the lateral pressure and vertical strain, and used these values to compute the apparent elastic modulus and apparent Poisson ratio. From their data the value of the ratio of lateral to vertical pressure, k, appeared to remain nearly constant for the high applied pressures used in their tests. The diameter of the grain column did not influence the results of the tests.

In tests in a shallow bin, Moore and Shaw (1952) found the lateral pressure exerted by wheat increased by approximately 45% after vibrating the bin. The vertical pressure on the bottom increased only about 5%.

Stewart (1964) measured the internal friction properties of sorghum grain with a triaxial compression test. He plotted the data in the form of the Mohr envelope of principal stresses to determine the internal friction and found that sorghum displayed an apparent cohesion in the range of 0.5 to 0.8 psi. While some of this cohesion may have been accounted for by instrument effect, Stewart felt some was caused by actual cohesion between the grains, due to grain moisture.

De Josselin (1959) in discussing a similar phenomenon in the Mohr diagram of dry sand stated, "--, an apparent cohesion caused by an interlocking effect which is produced by angularity of the grains."

3.5.2. Effect of applying a vertical load to pea beans

A stable arch system could be formed over a wider slit with a vertical load applied than with no applied load. The maximum width for flow arches with no load was about 0.45 in. (M = 1.8), but with 1 psi of applied load, the maximum width was increased to 0.55 in. (M = 2.2) for an initial arch system. The type of arch system formed in beans changed from flow to initial under the action of an applied load. Actually the effect of loading on the flow arch system could not be evaluated with this simple test stand because the grain did not flow evenly from all sections of the slit. Often the beans in one end would flow out rapidly causing the weights to be wedged against the side or end of the bin.

A slit width of 0.45 in. was selected for the tests with beans because at this width stable arch systems would be formed within the range of loading used in these tests. Flow arches formed in beans with no load about 10% of the trials at 0.45 in. slit width. All arch systems

formed in beans were not strong and those formed under a load nearly always failed when the load was removed.

The relationship between the depth of grain and the load necessary to form stable arch systems in 50% of the test runs is shown in Figure 3.4. This figure shows that the load necessary to produce stable arch systems increased rapidly with an increase in grain depth.

Earlier investigations, mentioned in Chapter 2, indicated that the effect at the bottom of a bin of a pressure applied to the surface diminishes as the height of the grain layer increases. The relationship found in this study and represented by the curve in Figure 3.4 could, therefore, be interpreted as representing a more constant stress state in the area surrounding the arch than at the surface. This verifies the logical assumption that the tendency for arch formation is influenced by the vertical and horizontal stress components in the area close to the opening.

Several methods for determining the vertical pressure at the bottom of a bin filled with a granular material under an applied load have been discussed earlier in this study. Three of these methods included some allowance for attenuation of the vertical pressure with an increase in depth of material. They will be compared here using the values of depth and surface load represented by the curve in Figure 3.4.

First, the method of Terzaghi (1943) was used. Using Equation 2.19, with the applied load taken from the curve in Figure 3.4, the vertical pressure on the center of the bottom of the bin was calculated

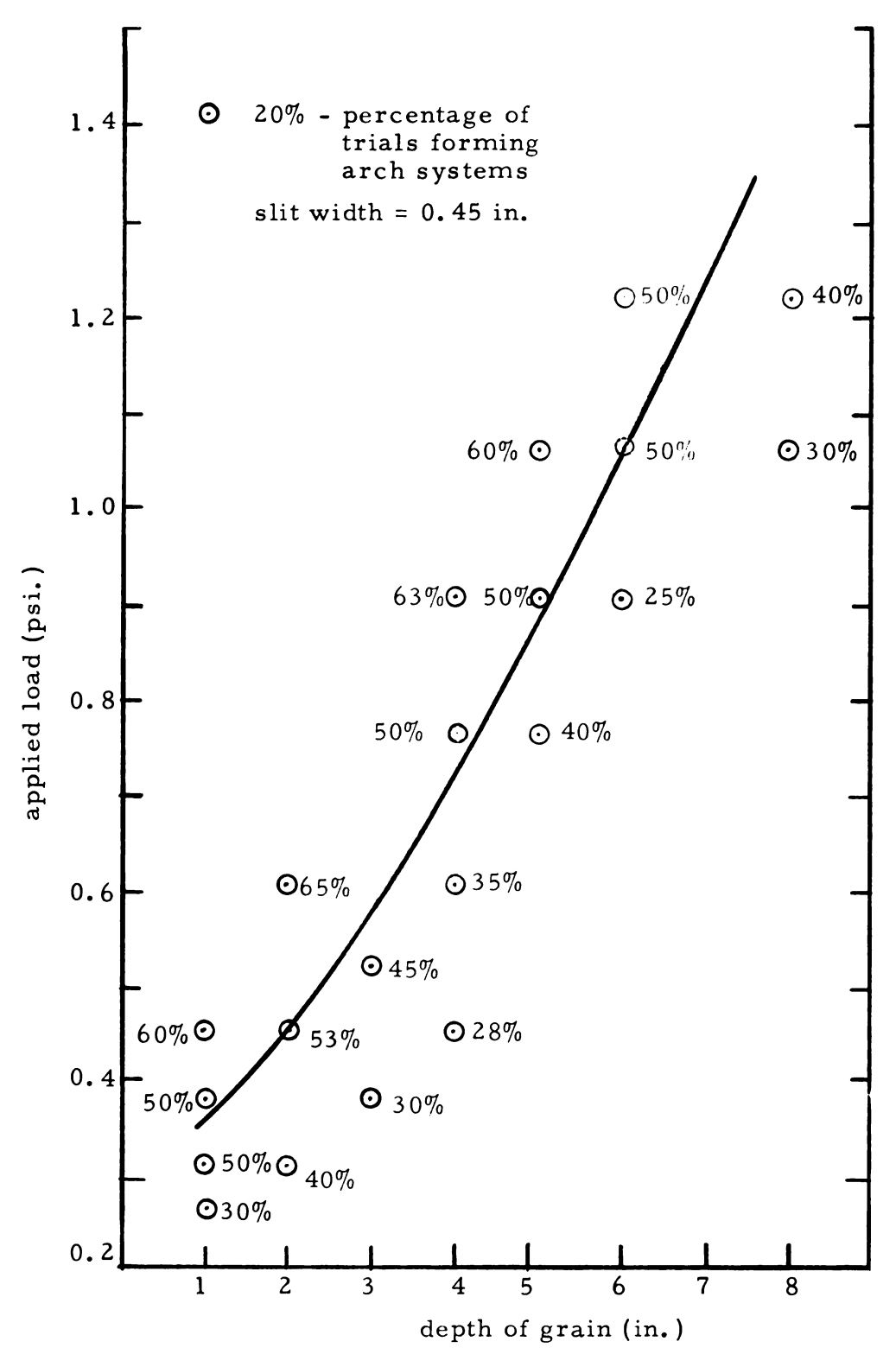


Figure 3.4. The load necessary to produce initial arches in 50% of tests with beans, for various depths of material.

for several depths of material. The values of the parameters used for the calculations were: c=0, c'=0, $\mu=0.5$, and $\mu'=0.4$. The results of these calculations are plotted in Figure 3.5.

Second, assuming that the stress distribution in the material in the model bin was similar to the stress distribution in a semi-infinite elastic material, the solution of Love (1929) (discussed briefly in Section 2.2.1) was used to calculate the vertical stress under the same conditions as were used above. Due to the symmetry of the point at which the computations were made, Poisson's ratio for the material did not affect the calculated vertical stress. These results are also plotted in Figure 3.5.

Last, the force system of Ross and Isaacs (1961) (discussed in Section 2.1.1) was extended to include the action of an applied load. Calculations were made for the same conditions as in the first two methods. The parameters used for these calculations were the values listed by Ross and Isaacs for soybeans. The results are also shown in Figure 3.5.

Since the tendency for arch formation was the same for all points on the curve in Figure 3.4, it might be assumed that the vertical stress around the arch should also be the same, i.e., represented by a horizontal line in Figure 3.5.

The results shown in Figure 3.5 indicate that a least two of the methods used did not accurately calculate the stress state which occurred in these tests. Terzaghi's method showed that the vertical pressure at the bottom of the bin was twice as great at an 8 in. depth as at a 2 in. depth of material for loads according to Figure 3.4.

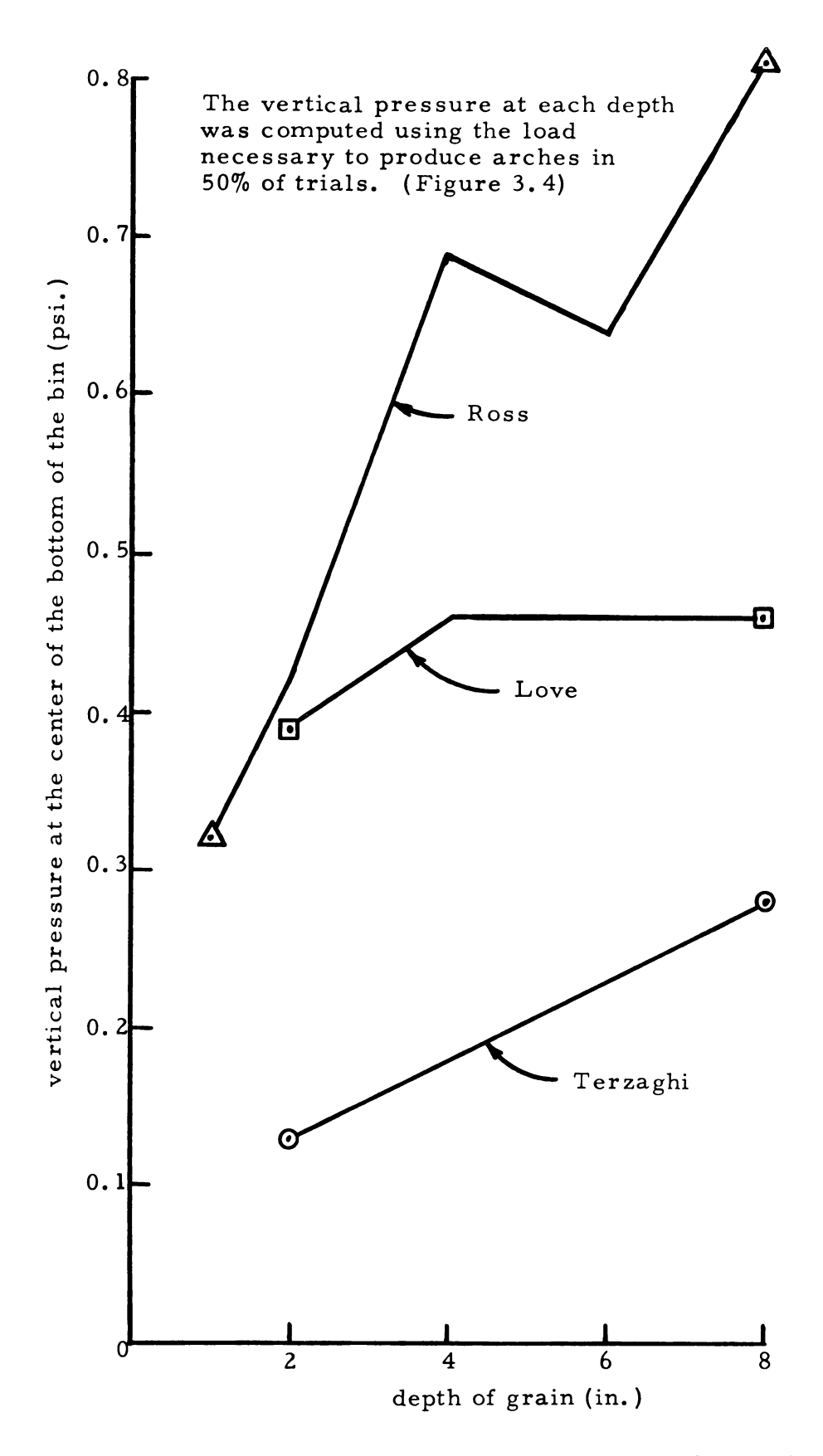


Figure 3.5. Vertical pressure on the bottom of the bin for various depths of beans, computed by three methods.

The method of Ross and Isaacs was not intended for this type of force system and gave poor results. Their method would probably be improved if an arching factor such as used by Trollope (1957) was included in the calculations.

Love's method gave the best results even though the conditions of these tests did not seem to fit his model.

The results of these three methods might have been improved if other values of the parameters had been chosen.

3.5.3. Effect of applying a vertical load to oat kernels

The arching properties of oat kernels were also changed by the application of a vertical load. Loading increased the rate of occurrence of initial arches at a given slit width and also increased the maximum width of a stable arch system. But more noticeably, loading increased the occurrence of flow arches.

A slit width of 0.55 in. was selected for the loading tests because this slit width gave about 5% formation of initial arches with compacted oat kernels without a load. Table 3.6 shows the effect of increasing loads on the formation of initial arches. This effect was much less than was observed in navy beans. The depth of grain under the load did not have much affect on the formation rate of this type of arch. When the load was removed from the grain mass, the arch system normally failed.

Table 3.6. Relation between applied load and the formation of initial arches for various depths of oats over a slit width of 0.55 in.

Load	Depth of grain (in.)			
(psi)	2	4	6	8
0.0	<5%	< 5%	< 5%	< 5%
0.5	10%	10%	5%	< 5%
0.65	10%	10%	10%	5%
1.0	30%	30%	30%	30%

Table 3.7 shows how loading affected the flow arches in oats. A load of 1.0 psi increased the formation of flow arches from less than 5% to nearly 100% of the trials. Loads of 0.5 psi caused flow arches to form in 50% of the trials.

Table 3.7. Relation between applied load and the formation of flow arches for various depths of oats over a slit width of 0.55 in.

Load	Depth of grain (in.)			
(psi)	4	6	8	
0.0	< 5%	< 5%	< 5%	
0.5	3 0%	50 %	60%	
0.65	50%	60%	80%	
1.0	100%	100%	100%	

As the depth of the material increased, the frequency of flow arch formations increased slightly. This was probably due to the greater amount of material which had to flow out during the tests at greater depths.

The application of the load seemed to prevent the reorientation of the oat kernels during flow, which increased the tendency to form arches.

3.5.4. Effect of applying a vertical load to sugar beet seed

The formation of stable arch systems in sugar beet seed was influenced by compacting the seeds and also by applying a vertical load to the seeds. Applying a load to the compacted seeds increased the arch widths to greater values than with no applied load. Figure 3.6 shows the relationship between the vertical load applied to a column of seeds and the percent of cases when stable arch systems formed.

The particles of the beet seed seemed to interlock during compacting, which increased the internal friction and cohesion of the compacted mass. Considering the equations derived in Section 2.1.4 for the failure strength, $F_{ta} = \mu_a F_{na}$, it can be seen that an increase in the internal friction and cohesion increases the strength of a material in the region of the minimum strength. The observed increase in arch width due to compacting indicated an increase in material strength, which agrees in general with the results of the yield criterion. Applying a load would increase the interlocking action between particles still more.

These results agree well with the results of Williams and Ross (1967). In tests with dried citrus pulp (a material which arches readily), they measured the vertical pressure at the bottom of the stacks of pulp and found that the pressure was much higher than predicted by Janssen's equation (see Section 2.2.1) or by the equations of Ross and Isaacs (see Section 2.1.1). Thus it appears that materials which have a tendency for particle interlocking and thus a high arching potential tend to act more like a unit mass than non-cohesive materials. By this action, forces are transmitted through the particle mass with less attentuation than through a mass of non-cohesive particles.

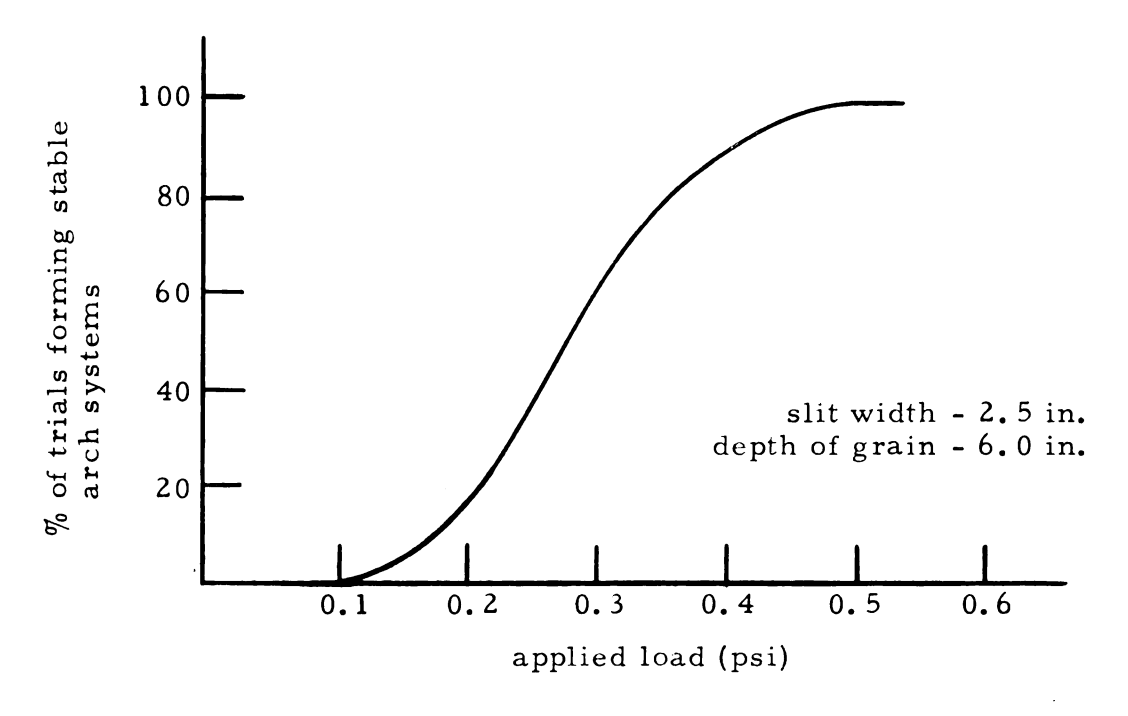


Figure 3.6. Effect of the applied load on the formation of stable arch systems in sugar beet seeds.

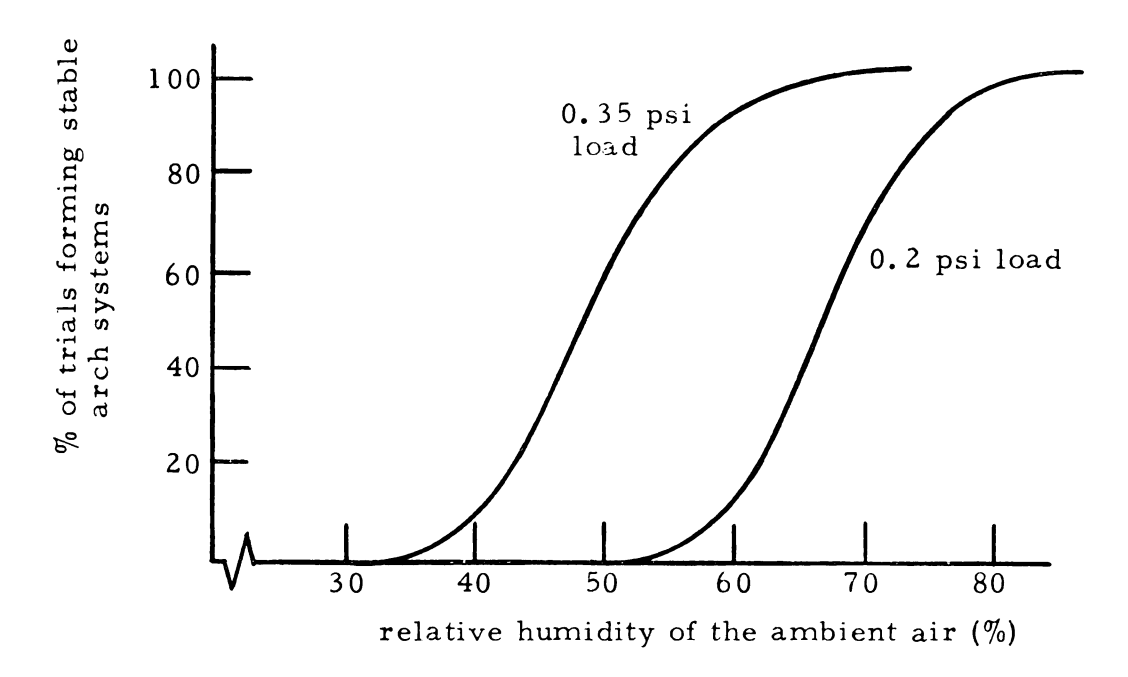


Figure 3.7. Effect of relative humidity on the formation of stable arch systems in sugar beet seeds.

3.6. Effect of Relative Humidity of the Ambient Air on Arch Formation

The relative humidity of the ambient air seemed to have an influence on the width of the stable arch systems which formed in sugar beet seeds. In these tests the relative humidity was kept constant at the desired value for three days before any tests were made. As the relative humidity increased from 30% to 80%, the width of a stable arch system in compacted seeds increased from 0.9 in. to 2.0 in. Figure 3.7 shows the relationship between the relative humidity of the air and the percentage of trials forming stable arch systems. Relative humidity did not noticeably affect the formation of arch systems (normally flow) in loosely poured seeds. The effect was also not so striking in the other materials tested.

The effect of the change in relative humidity may be explained by assuming a change in the surface properties of the seed. This would change the cohesion and interlocking between particles which probably occurs with seeds of this kind.

IV. CLOSURE

4.1. Conclusions

- 1. The observations made of arch formations indicate that for the materials used in this study, the orientation and shape of the particle affect the failure strength.
- 2. The primary-secondary arch structure was apparent in all materials with a nearly spherical particle shape.
- 3. The arching tendency of the granular materials used in this study increased when a vertical pressure was applied to the upper surface of the particle stack.
- 4. The arching tendency of sugar beet seed was greatly increased with an increase in its moisture content.
- 5. The yield criterion developed in this study was a function of shearing angle, particle shape and stacking arrangement of the particles and the internal friction and cohesion of the material.
- 6. Although no data was collected to test the yield criterion directly, the expected failure derived from the yield criterion agreed well with the failures observed in the arch tests.

4.2. Suggestions for Future Study

- 1. Experimentally measure the strength of granular materials at various shearing angles to determine the effect of
 - a. particle orientation
 - b. particle shape
 - c. particle stacking
 - d. coefficient of friction between particles.

- 2. Study the occurrence and nature of cohesion and interlocking between particles, including time effects on these properties.
- 3. Study the forces acting on elements along the stress-free surface of the arch. Can the yield criterion predict the critical arching width?
- 4. Irregular particles such as sand seem to have certain stacking arrangements which give very high strengths; can these high strength packing systems be described by the yield criterion and packing system developed here?
- 5. Measure the stress field in a particle mass. In a cohesive material such as preloaded sugar beet seed, is the assumption of an elastic body reasonable? If so, does the elastic body with a hole in the center mentioned in Section 2.2.3 give an accurate picture of the stress field? Does this stress field along with the yield criterion of this study describe the failure condition for arching?
- 6. Experimentally test materials with very small particles, such as clays to determine if the yield criterion of this study describes the shearing strength of these materials.

REFERENCES

Allan, W. (1890). Theory of Arches. D. Van Nostrand Company, New York. 121 pp.

Airy, Wilfrid (1897). The pressure of grain. Proceedings of the Institution of Civil Engineers 131: 347-358.

Aytaman, Vedat (1960). Causes of "hanging" in ore chutes. Canadian Mining Journal 81: 77-81.

Aytaman, Vedat (1960). Study of particle arches under exerted pressure. Canadian Mining Journal 81: 71-75.

Beverloo, W. A., H. A. Leniger, and J. Van de Velde (1961). The flow of granular solids through orifices. Chemical Engineering Science 15: 260-269.

Brown, R. L. and J. C. Richards (1959). Exploratory study of the flow of granules through apertures. Transactions of the Institution of Chemical Engineers 37: 108-119.

Brown, R. L. and J. C. Richards (1960). Profile of flow of granules through apertures. Transactions of Institution of Chemical Engineers 38: 243-256.

Carr, Ralph L. Jr. (1965). Evaluating flow properties of solids. Chemical Engineering 72: 69-72.

Caughey, R. A., C. W. Tooles and A. C. Scheer (1951). Lateral and Vertical Pressure of Granular Material in Deep Bins. Iowa Engineering Experiment Station Bulletin 172, 32 pp.

Collins, S. H. and Paul K. K. Yin (1965). A model study of the bin flow of dry grain. Canadian Agricultural Engineering 7: 14-16.

DeJosselin DeJong, G. (1959). Statics and Kinematics in the Failable Zone of a Granular Material. Uitgeverij Waltman, Delft. 117 pp.

Delaplaine, John W. (1956). Forces acting in flowing beds of solids. American Institute of Chemical Engineers 2: 127-138.

Deming, W. Edwards and Arnon L. Mehring (1929). The gravitational flow of fertilizers and other comminuted solids. Industrial and Engineering Chemistry 21: 661-665.

Deresiewicz, H. (1958). Mechanics of granular material. pp. 233-303, in <u>Advances in Applied Mechanics</u>, Volume 5. Academic Press, Inc., New York. 459 pp.

- Farouki, C. T. and Hans F. Winterkorn (1964). Mechanical properties of granular systems. Highway Research Record No. 52, 10-58.
- Fowler, R. T. and J. R. Glastonbury (1959). The flow of granular solids through orifices. Chemical Engineering Science 10: 150-156.
- Franklin, F. C. and L. N. Johanson (1955). Flow of granular material through a circular orifice. Chemical Engineering Science 4: 119-129.
- Fröhlich, O. K. (1934). Die Druckverteilung in der Silozelle und im Baugrunde. Beton u. Eisen 17: 268-272.
- Hall, C. W. (1957). <u>Drying Farm Crops</u>. Edwards Brothers, Inc., Ann Arbor. 336 pp.
 - Hall, C. W. (1961). Storage of farm crops. Chapt. 50, pp. 672-694, in C. B. Richey, Ed. Agricultural Engineers' Handbook. McGraw-Hill, Inc., New York. 880 pp.
 - Hildebrand, F. B. (1956). <u>Introduction to Numerical Analysis</u>. McGraw-Hill, Inc., New York. 511 pp.
 - Isaacson, J. D. (1963). Mathematical analysis of static and dynamic lateral pressure in the infinite upright flat-bottomed deep grain bin. Thesis for the degree of PhD., Michigan State University, East Lansing. (Unpublished).
 - Jamieson, J. A. (1904). Grain pressures in deep bins. Engineering News 51: 236-243.
 - Janssen, H. A. (1895). Versuche über Getreidedruck in Silozellen. Zeitschrift des VDI 39: 1045-1049.
 - Jenike, A. W. and R. T. Shield (1959). On the plastic flow of Coulomb solids beyond original failure. Journal of Applied Mechanics 26: 599-602.
 - Jenike, A. W. (1961). Gravity flow of bulk solids. Utah Engineering Experiment Station Bulletin 108, Salt Lake City. 309 pp.
 - Ketchum, Milo S. (1919). The Design of Walls, Bins, and Grain Elevators. McGraw-Hill, Inc., New York. 554 pp.
 - Khan, A. (1966). Research engineer, International Rice Institute, Manila, Philippines. Personal Correspondence, December 20.
 - Kramer, Harold A. (1944). Factors influencing the design of bulk storage bins for rough rice. Agricultural Engineering 25: 463-466.
 - LaForge, R. M. (1962). Recent studies concerning the flow of granular bulk materials. Engineering Experiment Station Bulletin 27, Knoxville, Tennessee, 26 pp.

Langmaid, R. N. and H. E. Rose (1957). Arch formation in non-cohesive granular materials. Institute of Fuel Journal 30: 166-172.

Laszlo, F. (1962). Stability of granular masses. Journal of the Engineering Mechanics Division, Proceedings of the American Society of Civil Engineers 88: 115-140.

Lee, Chesman A. (1963). Hopper design up to date. Chemical Engineering 70: 75-78.

Lenczner, D. (1966). Cohesive arching of bulk materials in bunkers and silos. Civil Engineering and Public Works Review 61: 1393-1396.

Little, R. W. (1966). Notes handed out in MMM 813, Winter Quarter, Michigan State University, East Lansing.

Lorenzen, Robert T. (1957). Effect of moisture content on mechanical properties of small grains. Thesis for the degree of M.S., University of California, Davis. (Unpublished)

Love, A. E. H. (1929). The stress produced in a semi-infinite solid by pressure on part of the boundary. Royal Society of London Philosophical Transactions 228: 377-420.

Lufft, Eckhardt (1904). Tests of grain pressure in deep bins at Buenos Aires, Argentina. Engineering News 52: 531-532.

Menear, J. R. and R. D. Holdren (1965). Handling, storing, drying wafered hay in humid areas. Transactions of American Society of Agricultural Engineers 8: 256-258 and 263.

Mogami, Takeo (1965). A statistical theory of mechanics of granular materials. Journal of the Faculty of Engineering, University of Tokyo, Series B. 28: 66-79.

Mogami, Takeo (1966). Angle of internal friction of the granular material and a simple transient phenomenon. Daboku Gakkai, Transactions of the Japan Society of Civil Engineers 128: 53-62.

Moore, Raymond L. and J. R. Shaw (1952). Pressures in a shallow rectangular bin. Transactions of American Society of Civil Engineers 117: 370-382.

National Agricultural Advisory Service (1967). Moist grain silo management. Farm Mechanization and Buildings 19: 20.

O'Callaghan, J. R. (1960). Internal flow in moving beds of granular material. Journal of Agricultural Engineering Research 5: 200-217.

Rausch, J. M. (1948). Gravity flow of solid beds in vertical towers. Thesis for the degree of PhD., Princeton University, Princeton, N.J. (Unpublished).

Richmond, O. and G. C. Gardner (1962). Limiting spans for arching of bulk materials in vertical channels. Chemical Engineering Science 17: 1071-1078.

Roberts, Isaac (1884). Determination of the vertical and lateral pressures of granular substances. Engineering News, April 1883, 151-159.

Rose, H. E. and Tatsuo Tanaka (1959). Rate of discharge of granular materials from bins and hoppers. The Engineer 208: 465-469.

Ross, I. J. and G. W. Isaacs (1961). Forces acting in stacks of granular materials. Transactions of the American Society of Agricultural Engineers 4: 92-96.

Saul, Robert A. (1953). Measurement of grain pressures on bin walls and floors. Agricultural Engineering 34: 231-234.

Schlack, A. L. and R. W. Little (1964). Elastostatic problem of a perforated square plate. Journal of the Engineering Mechanics Division, Proceedings of the American Society of Civil Engineers 90: 171-188.

Simons, J. W. and W. W. Hare (1965). Grain drying and storage studies in Southwest Georgia. U. S. Department of Agriculture Technical Bulletin 1342. 58 pp.

Smith, Julian C. (1955). Design a hopper that won't arch. Chemical Engineering 62: 167-168.

Sokolovskii, V. V. (1965). Statics of Granular Media. Pergamon Press, New York. 270 pp.

Stewart, Bill R. (1964). Effect of moisture content and specific weight on the internal friction properties of sorghum grain. ASAE paper No. 64-804.

Terzaghi, Karl (1936). Stress distribution in dry and in saturated sand above a yielding trap door. Proceeding of International Conference on Soil Mechanics, Cambridge, Mass. Vol. I, 307-311.

Terzaghi, Karl (1943). Theoretical Soil Mechanics. John Wiley and Sons, Inc., New York. 510 pp.

Thompson, T. R. (1965). Elastostatic problem of a perforated rectangular plate. Thesis for the degree of M.S., Oklahoma State University, Stillwater. (Unpublished).

Timoshenko, S. and J. N. Goodier (1951). Theory of Elasticity. McGraw-Hill, Inc., New York. 506 pp.

Trollope, D. H. (1957). The systematic arching theory applied to the stability analysis of embankments. Proceedings of the Fourth International Conference on Soil Mechanics and Foundation Engineering, London, Vol. II, 382-388.

Turitzin, Alexander M. (1963). Dynamic pressure of granular material in deep bins. Journal of Structural Division, Proceedings of the American Society of Civil Engineers 89: 49-73.

Welschof, Gerhard (1961). Beitrag zur Messung der Ausflussmengen körniger Güter mit Blenden und Düsen. Landtechnische Forschung 2: 138-141.

Williams, E. J. and I. J. Ross (1967). The vertical pressure acting on the bottom of confined stacks of dried citrus pulp. ASAE paper number 67-924, 19 pp.

